Pakistan Journal of Statistics and Operation Research

A Novel Insurance Claims (Revenues) Xgamma Extension: Distributional Risk Analysis Utilizing Left-Skewed Insurance Claims and Right-Skewed Reinsurance Revenues Data with Financial PORT-VaR Analysis

Haitham M. Yousof[1], Mahmoud Afshari[2], Morad Alizadeh[2], Vahid Ranjbar[3], R. Minkah[4], Mohamed S. Hamed[5,1] and Moustafa Salem[6]

* Corresponding Author

[1]Department of Statistics, Mathematics and Insurance, Benha University, 13518, Egypt; haitham.yousof@fcom.bu.edu.eg
[2]Department of Statistics, Persian Gulf University, Bushehr, 75169, Iran; moradalizadeh78@gmail.com & afshar@pgu.ac.ir
[3]Department of Statistics, Golestan University, Gorgan, Iran; vahidranjbar@gmail.com
[4]Department of Statistics and Actuarial Science, School of Physical and Mathematical Sciences, College of Basic and Applied Sciences, University of Ghana, Accra, Ghana; rminkah@ug.edu.gh
[5]Department of Business Administration, Gulf Colleges, KSA (E-mail: mssh@gulf.edu.sa).
[6]Department of Applied Statistics, Damanhour University, Egypt; moustafasalemstat@com.dmu.edu.eg

Abstract

The continuous probability distributions can be successfully utilized to characterize and evaluate the risk exposure in applied actuarial analysis. Actuaries often prefer to convey the level of exposure to a certain hazard using merely a numerical value, or at the very least, a small number of numbers. In this paper, a new applied probability model was presented and used to model six different sets of data. About estimating the risks that insurance companies are exposed to and the revenues of the reinsurance process, we have analyzed and studied data on insurance claims and data on reinsurance revenues as an actuarial example. These actuarial risk exposure functions, sometimes referred to as main risk actuarial indicators, are unquestionably a result of a particular model that can be explained. Five crucial actuarial indicators are used in this study to identify the risk exposure in insurance claims and reinsurance revenues. The parameters are estimated using techniques like the maximum product spacing, maximum-likelihood, and least square estimation. Monte Carlo simulation research is conducted under a specific set of conditions and controls. Additionally, five actuarial risk indicators including the value-at-risk, tail-variance, tail value-at-risk, tail mean-variance, and mean of the excess loss function, were utilized to explain the risk exposure in the context of data on insurance claims and reinsurance revenue. The peak over a random threshold value-at-risk (PORT-VaR) approach and value-at-risk estimate are taken into account and contrasted for detecting the extreme financial insurance peaks.

Key Words: Cullen-Frey plot; Maximum Product Spacing; Financial Peaks; Mean Excess Loss Function; Risk exposure; Risk indicators; Value-at-risk; Peak Over Random Threshold; XGamma model

1.Introduction

Elbatal et al. (2024) introduced a novel and significant probability model tailored for the analysis of losses and revenues. Their model incorporated entropy-based measures and provided valuable insights through applications and case studies, particularly in the contexts of value-at-risk (VaR) modeling and mean of order-P (MOO_P) analysis. Despite its theoretical contributions, the model proposed by Elbatal et al. (2024) demonstrates certain limitations, specifically, a lack of flexibility in its probability density function (PDF) and hazard rate function (HRF). These structural constraints hinder its ability to accurately capture the diverse and often complex behavior observed in real-world financial data involving losses and revenues. This notable gap in the existing literature serves as the key motivation behind our work. In response, we propose a new, more adaptable statistical model designed to overcome these shortcomings and provide a more robust framework for modeling and interpreting financial and actuarial risks and returns.

The actuarial assessment of the potential loss that could occur in the future because of a given actuarial action or occurrence is known as the risk exposure. As part of the actuarial analysis of the business's exposure to risk, actuarial risks are frequently ranked according to their probability of happening in the future multiplied by the loss that would result if they did. By rating the risk of expected losses in the future, insurance (and reinsurance) companies can distinguish between little and major losses. Speculative risks frequently lead to losses including breaking rules, losing brand value, having security flaws, and having liability problems. The chance of a risk happening and the total loss if it does may often be multiplied to get the risk exposure. On the other hand, a lot of work has gone into applying several statistical methods, such as the continuous distributions and time series analysis, to analyze historical insurance data (see Rasekhi et al. (2022) and Salem et al. (2023), Shrahili et al. (2021), Mohamed et al. (2022), Yousof et al. (2023a,b,c), Yousof et al. (2024a,b) and Mohamed et al. (2024)).

Recent years have seen an increase in the usage of continuous distributions, especially those with large tails, to reflect actual data from the insurance or reinsurance industries. In many real applications, such as economics, engineering, risk management, dependability, and actuarial sciences, actuarial data is modelled using continuous heavy-tailed probability distributions. The data sets for insurance claims and reinsurance may be unimodal (bimodal) left-skewed, unimodal (bimodal) right-skewed, or both with large tails. Reinsurance is the term used in actuarial literature to describe the coverage an insurance organization obtains from another insurance provider to safeguard itself (at least in part) against the potential of a sizable claim. Stop-loss insurance, insurance for insurers, and reinsurance are terms that are frequently used to describe reinsurance. Reinsurance is a term used to describe the process by which insurers, through some form of agreement, transfer a portion of their risk portfolios to other parties to reduce the likelihood that they may face a significant financial burden because of an insurance claim. The process of reinsurance can be used by reinsurance seekers or ceding businesses to expand their ability to take on any form of risk. Financial reinsurance is a tactic used by life insurance carriers to balance their returns and keep a profit. This approach may be used by other firms who want to increase their profits without considerably raising their risk. Several recent studies have introduced innovative statistical models tailored for actuarial, reliability, and extreme value analysis. Ibrahim et al. (2025) proposed a novel Fréchet-Poisson model with various estimation methods, applied effectively in strength-stress reliability under extreme data. Ramaki et al. (2025) developed the Weighted Flexible Weibull model, demonstrating its suitability for modeling extreme events in reliability and risk studies. Ibrahim et al. (2025) also introduced a new Reciprocal Weibull distribution, highlighting its adaptability for medical and reliability data along with a sequential sampling plan. In another contribution, Alizadeh et al. (2025) presented a new Weighted Lindley model, showcasing its ability to handle extreme historical insurance claims efficiently. Das et al. (2025) focused on economic data by applying a Laplace distribution to model house price peaks, offering insights into Value-at-Risk (VaR) analysis. Ibrahim et al. (2025) further extended inverse Weibull modeling, providing comprehensive estimation techniques and real-life applications. Abonongo et al. (2025) developed an accelerated failure time model with a focus on colon cancer data, contributing to survival analysis and model validation techniques. Another study by Ibrahim et al. (2025) introduced an extended discrete model for actuarial data, particularly useful in financial automobile claims and VaR assessment. AlKhayyat et al. (2025) contributed a Rao-Robson-Nikulin goodness-of-fit test adapted for censored and uncensored data, integrating both classical and Bayesian estimation frameworks. Hashempour et al. (2024) explored the Weighted Xgamma model, emphasizing its risk analysis potential and flexible structure for complex datasets. Lastly, Alizadeh et al. (2024) proposed the Extended Gompertz model, integrating mean-of-order-P measures and threshold-based risk evaluation under extreme stress data scenarios.

In this study, we present a probability model for projecting and analyzing insurance claims and reinsurance enterprises' revenues, accounting for both these crucial factors and current global trends in insurance and reinsurance. However, any actuarial model stands out due to the simple procedures and good level of forecast accuracy. As part of a review of the business's risk exposure, risks are often rated according to their tendency to occur in the future multiplied by the potential loss if they did. The company can distinguish between minor and substantial losses by estimating the likelihood of future expectations losses. Speculative risks typically result in losses, such as breaking rules, losing brand value, having security flaws, and having liability problems. Time series analysis or continuous distributions have been intensively investigated for the study of historical insurance data. Recently, continuous distributions, particularly those with long tails, have been employed by actuaries to represent actual insurance data. Engineering, risk management, dependability, and the actuarial sciences are just a few of the real applications where real data has been simulated using continuous heavy-tailed probability distributions. The insurance data sets' skewness can be either left, right, or right with massive tails. Actuaries typically look for heavy-tailed distributions when modelling data that relates to actuarial and business risk issues. In this paper, we introduce a novel class of heavy-tailed distributions for

simulating data in the financial sciences. Many applied studies have studied reinsurance data in one way or another: for some applications of spectral and autoregressive integrated moving average analysis, see Venezian and Leng (2006), for the dynamics of unemployment reinsurance revenues with an application, see Mohammadi and Rich (2013). The autoregressive integrated moving average model was used by Hafiz et al. (2021) to forecast insurance penetration rates in Nigeria, and Kumar et al. (2020) to forecast motor insurance claim amounts. It is worth noting that the consideration of such important reinsurance data is extremely rare in the actuarial literature. While there are studies that dealt with the issue of insurance claims in general. In this paper, we will cover this flaw in the literature by relying on reinsurance data in analyzing and evaluating the risks faced by reinsurance companies, see Hamed et al. (2022), Hamedani et al. (2023), Hashempour et al. (2024a, b) for more relevant works.

Distributions based on probabilities might be able to explain risk exposure effectively. Usually, one number, or at the very least, a limited number of numbers, are used to describe the amount of risk exposure. Commonly known as crucial critical risk indicators, these risk exposure numbers, which are undeniably the outcome of a specific model, reflect the importance of the key risk indicators (KRIs) they represent (see Artzner (1999)). Actuaries and risk managers can learn from such KRIs how exposed a company is to various dangers. The tail-value-at-risk (TVaR), value-at-risk (VaR), conditional-value-at-risk (CVaR) tail Mean-Variance (TMV) and tail variance (TV), are just a few of the KRIs that can be considered and studied. Specific to the quantile distribution of aggregate losses is the VaR. Most of the time, actuaries and risk managers focus on estimating the likelihood of a negative result, which can be calculated using the VaR indicator at a specific probability/confidence level. The amount of money needed to deal with such probable negative effects is often estimated using this indicator. Actuaries, policymakers, investors, and rating agencies are concerned about the insurance company's capacity to handle. For the purpose of analyzing and evaluating the risks that reinsurance companies are exposed to, we will present a new flexible distribution with a heavy tail on the right and left side also called the novel odd log-logistic XGamma (NOLLX) distribution, the new model is derived based on the the XGamma (X) model (see Sen et al. (2016)) and considered as applicable extension which can be applied in the actuarial sciences.

The XGamma model is applied successfully to time-to-event data set, and its different properties are studied. Then, following Sen et al. (2016), Yadav et al. (2021b), introduced a new monotone failure rate exponentiated XGamma model. Sen et al. (2018) presented a new compound XGamma model called quasi XGamma-Poisson distribution, The XGamma G family is a new family for censored regression modelling and applications that [cor] examine using Sen et al. (2016)'s XGamma model, Yadav et al. (2021a) presented the inverse XGamma distribution. The Nikulin-Rao-Robson goodness-of-fit test was used to statistically validate by Yadav et al. (2022) under the XGamma exponential model using both complete and censored samples with various estimating techniques. For more details see Bantan et al. (2020) (for the half-logistic XGamma model), Para et al. (2020) (for the Poisson XGamma model). Generally, the XGamma distribution has been used to analyze failure time data as well as for modelling data in reliability, biology, insurance and finance over the past decades. The XGamma (Sen et al. (2016)) distribution has been used to analyze failure time data as well as for modelling data in reliability, biology, insurance and finance over the past decades. Loubna et al. (2024) presented a quasi-xgamma frailty model with survival analysis under heterogeneity problem. The PDF and cumulative distribution function (CDF) of the XGamma distribution with parameter (λ) are, respectively, given by

$$w_\lambda(\boldsymbol{x}) = \frac{1}{(\lambda+1)\,exp(\lambda\boldsymbol{x})}\left(1 + 0.5\,\frac{\lambda}{\boldsymbol{x}^{-2}}\right)\lambda^2 \text{ and } W_\lambda(\boldsymbol{x}) = 1 - \frac{1}{exp(\lambda\boldsymbol{x})}\phi_\lambda(\boldsymbol{x})|_{\boldsymbol{x}>0,\lambda>0},$$

where $\phi_\lambda(\boldsymbol{x}) = \left(\frac{0.5\eta}{\lambda+1}\boldsymbol{x}^2 + \frac{\lambda}{\lambda+1}\boldsymbol{x} + 1\right)$. The proposed distribution can be quite flexible in terms of the hazard rate function and PDF, and it can be helpful in lifetime data analysis, actuarial science, finance, bioscience, and telecommunications. The odd log-logistic XGamma (GOLLX) distribution, a new generalization of the XGamma distribution, is presented for the desired distribution risk analysis using the unimodal right-skewed reinsurance revenues and the unimodal left-skewed insurance claims payments data with Peaks-Over Random Threshold (PORT) analysis. The CDF of the GOLLX is

$$F_{\underline{V}}(\boldsymbol{x}) = \{[1 - \mathcal{U}(\boldsymbol{x};\lambda)]^\alpha + [\mathcal{U}(\boldsymbol{x};\lambda)]^\alpha\}^{-\beta}[1 - \mathcal{U}(\boldsymbol{x};\lambda)]^{\beta\alpha}, \tag{1}$$

where α, β are two extra shape parameters and $\mathcal{U}(\boldsymbol{x};\lambda) = \frac{\phi_\lambda(\boldsymbol{x})}{exp(\lambda\boldsymbol{x})}$. Then, the corresponding PDF of the GOLLX distribution is given by

$$f_{\underline{V}}(\boldsymbol{x}) = \frac{\beta\alpha\lambda^2}{\lambda+1}\frac{\left(1+0.5\frac{\lambda}{\boldsymbol{x}^{-2}}\right)[\phi_\lambda(\boldsymbol{x})]^{\beta-1}}{[1-\mathcal{U}(\boldsymbol{x};\lambda)]^{1-\beta\alpha}} exp(-\lambda\beta\boldsymbol{x})\{[1-\mathcal{U}(\boldsymbol{x};\lambda)]^{\alpha}+[\mathcal{U}(\boldsymbol{x};\lambda)]^{\alpha}\}^{-\beta-1}. \quad (2)$$

Figure 1 shows charts for the PDFs of the NOLLX distribution for various parameter values (see the plots of the first row). Figure 1 shows charts for the HRFs of the NOLLX distribution for various parameter values (the plots of the second row). Due to Figure 1 (plots of the first row), The NOLLX model's density can have an asymmetric right-skewed distribution that has one peak and a heavy tail to the right, or it can have an asymmetric right-skewed distribution that has no peaks and a heavy tail to the right. Due to Figure 1 (plots of the second row), the HRF of the NOLLX model can take on several different forms, including increasing monotonically HRF, monotonically decreasing HRF, U-HRF (bathtub), upside-down, and upside-down-bathtub. The flexibility of new PDFs and their associated HRFs provides a significant advantage in statistical modelling procedures and real-life applications in several fields including medicine, engineering, finance and insurance. All these advantages were strong inducements for us to present the new model and the related method of risk evaluation and analysis.

2. Some properties

Using generalized binomial expansion and geometric expansion we can obtain

$$F(\boldsymbol{x};\alpha,\beta,\lambda) = \sum_{\varsigma,l=0}^{\infty}\sum_{\kappa=0}^{\varsigma}\sum_{\hbar=0}^{\varsigma-\kappa} w_{\varsigma,\kappa,l,\hbar}\, G(\boldsymbol{x};\lambda)^{\alpha(\beta+\hbar)+l} \quad (3)$$

where $w_{\varsigma,\kappa,l,\hbar} = (-1)^{\varsigma+\kappa+l+\hbar}\binom{-\beta}{\varsigma}\binom{\varsigma}{\kappa}\binom{\alpha\kappa}{l}\binom{\varsigma-\kappa}{\hbar}$. Equation (3) shows that CDF of GOLLX can expressed as a linear combination of exponentiated XGamma (EXG) distribution, similarly

$$f(\boldsymbol{x};\alpha,\lambda) = \sum_{\varsigma,l=0}^{\infty}\sum_{\kappa=0}^{\varsigma}\sum_{\hbar=0}^{\varsigma-\kappa} q^* w_{\varsigma,\kappa,l,\hbar}\, g(\boldsymbol{x};\lambda)G(\boldsymbol{x};\lambda)^{q^*-1}\,|_{q^*=\alpha(\hbar+\beta)+l}. \quad (4)$$

Equation (4) shows that CDF of GOLLX can expressed as a linear combination of EXG. Now, we can derive some mathematical properties of the new model based on EXG distribution. Let $\mu_n = E(X^n) = \int_0^\infty \boldsymbol{x}^n f(\boldsymbol{x})d\boldsymbol{x}$ denote the n-th moment of X. Let us first define and compute

$$A(\zeta_1,\zeta_2,\zeta_3;\lambda) = \int_0^\infty \boldsymbol{x}^{\zeta_1}(1+0.5\lambda\boldsymbol{x}^2)[1-\phi_\lambda(\boldsymbol{x})]^{\zeta_2} exp(-\zeta_3\boldsymbol{x})\, d\boldsymbol{x},$$

where $\zeta_1 > 0, \zeta_2 \geq 1, \zeta_3 \geq 0$ are real numbers. After using generalized binomial expansion and multinomial expansion we obtain

$$A(\zeta_1,\zeta_2,\zeta_3;\lambda) = \sum_{\xi=0}^{\infty}\sum_{(\xi_1,\xi_2)\in A} v_{\xi,\xi_1,\xi_2}\left[\frac{1}{(\lambda\xi+\zeta_3)^{p^*+1}}\Gamma(p^*+1)+\frac{0.5\lambda}{(\lambda\xi+\zeta_3)^{p^*+3}}\Gamma(p^*+3)\right]|p^* = \zeta_1+\xi_1+2\xi_2,$$

and

$$v_{\xi,\xi_1,\xi_2} = \frac{(-1)^{\xi}(\lambda+1)^{-\xi_1-\xi_2}\lambda^{\xi_1+2\xi_2}\xi!\binom{\zeta_3}{\xi}}{2^{\xi_2}(\lambda+1)^{\xi_1+\xi_2}\xi_1!\,\xi_2!\,(\xi-\xi_1!-\xi_2!)}, A = \{(\xi_1,\xi_2)|0\leq\xi_1\leq\xi, 0\leq\xi_2\leq\xi, 0\leq\xi_1+\xi_2\leq\xi\},$$

and $\Gamma(a) = \int_0^\infty \boldsymbol{x}^{a-1} exp(-\boldsymbol{x})\, d\boldsymbol{x}$ (for any $a > 0$) denote the gamma function. Then using equation (pdfmixture), we obtain

$$\mu_n = \frac{\lambda^2}{\lambda+1}\sum_{\varsigma,l=0}^{\infty}\sum_{\kappa=0}^{\varsigma}\sum_{\hbar=0}^{\varsigma-\kappa}(\alpha(\hbar+1)+l)w_{\varsigma,\kappa,l,\hbar}A(n,q^*-1,\lambda;\lambda).$$

The moment generating function (MGF) of X using equation (4), can be obtained as

$$M_X(t) = \frac{\lambda^2}{\lambda+1}\sum_{\varsigma,l=0}^{\infty}\sum_{\kappa=0}^{\varsigma}\sum_{\hbar=0}^{\varsigma-\kappa} q^* w_{\varsigma,\kappa,l,\hbar}A(n,q^*-1,\lambda-t;\lambda)$$

Let $m_n(y) = E(X^n|_{[X\leq y]}) = \frac{1}{F(y)}\int_0^y f(\boldsymbol{x})\,\boldsymbol{x}^n d\boldsymbol{x}$ denote the n th incomplete moment of X. Let us first define and compute

$$B(\zeta_1,\zeta_2,\zeta_3;y,\lambda) = \int_0^y \boldsymbol{x}^{\zeta_1}(1+0.5\lambda\boldsymbol{x}^2)[1-\mathcal{U}(\boldsymbol{x};\lambda)]^{\zeta_2} exp(-\zeta_3\boldsymbol{x})\, d\boldsymbol{x},$$

where $\zeta_1 > 0, \zeta_2 \geq 1, \zeta_3 \geq 0$ are real numbers. After using generalized binomial expansion and multinomial expansion we obtain

$$B(\zeta_1, \zeta_2, \zeta_3; \mathcal{y}, \lambda) = \sum_{\xi=0}^{\infty} \sum_{(\xi_1,\xi_2)\in A} v_{\xi,\xi_1,\xi_2} \left\{ \begin{matrix} \frac{1}{(\lambda\xi + \zeta_3)^{p^*+1}} \gamma((p^*+1), \mathcal{y}(\lambda\xi + \zeta_3)) \\ + \frac{0.5\lambda}{(\lambda\xi + \zeta_3)^{p^*+3}} \gamma((p^*+3), \mathcal{y}(\lambda\xi + \zeta_3)) \end{matrix} \right\}$$

where $\gamma(v, \boldsymbol{x}) = \int_0^{\boldsymbol{x}} t^{v-1} e^{-t} dt$ represent the lower incomplete gamma function. Using equation (4), we can write

$$m_n(\mathcal{y}) = \frac{\lambda^2}{(\lambda+1)F(\mathcal{y})} \sum_{\varsigma,l=0}^{\infty} \sum_{\kappa=0}^{\varsigma} \sum_{\hbar=0}^{\varsigma-\kappa} q^* w_{\varsigma,\kappa,l,\hbar} B(n, q^*-1, \lambda; \mathcal{y}, \lambda).$$

Figure 2 below presents the plots of the expectation (top left), variance (top right), skewness (bottom left) and kurtosis (bottom right) for the GOLLX distribution using selected values of α and β for λ = 2. These plots show the wide flexibility of the new model in this regard.

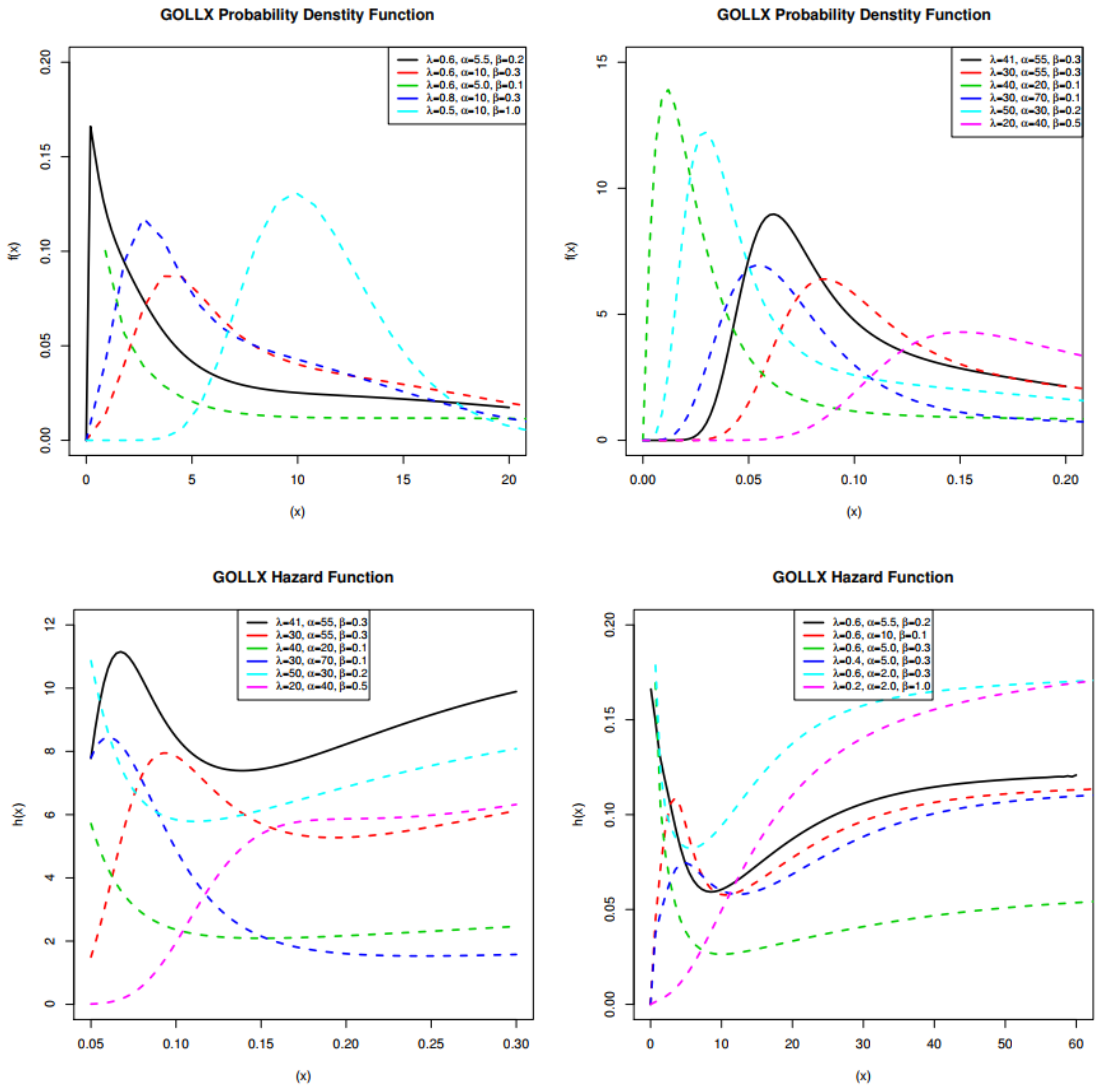

Figure 1: Different shapes of GOLLX pdf and Hazard function.

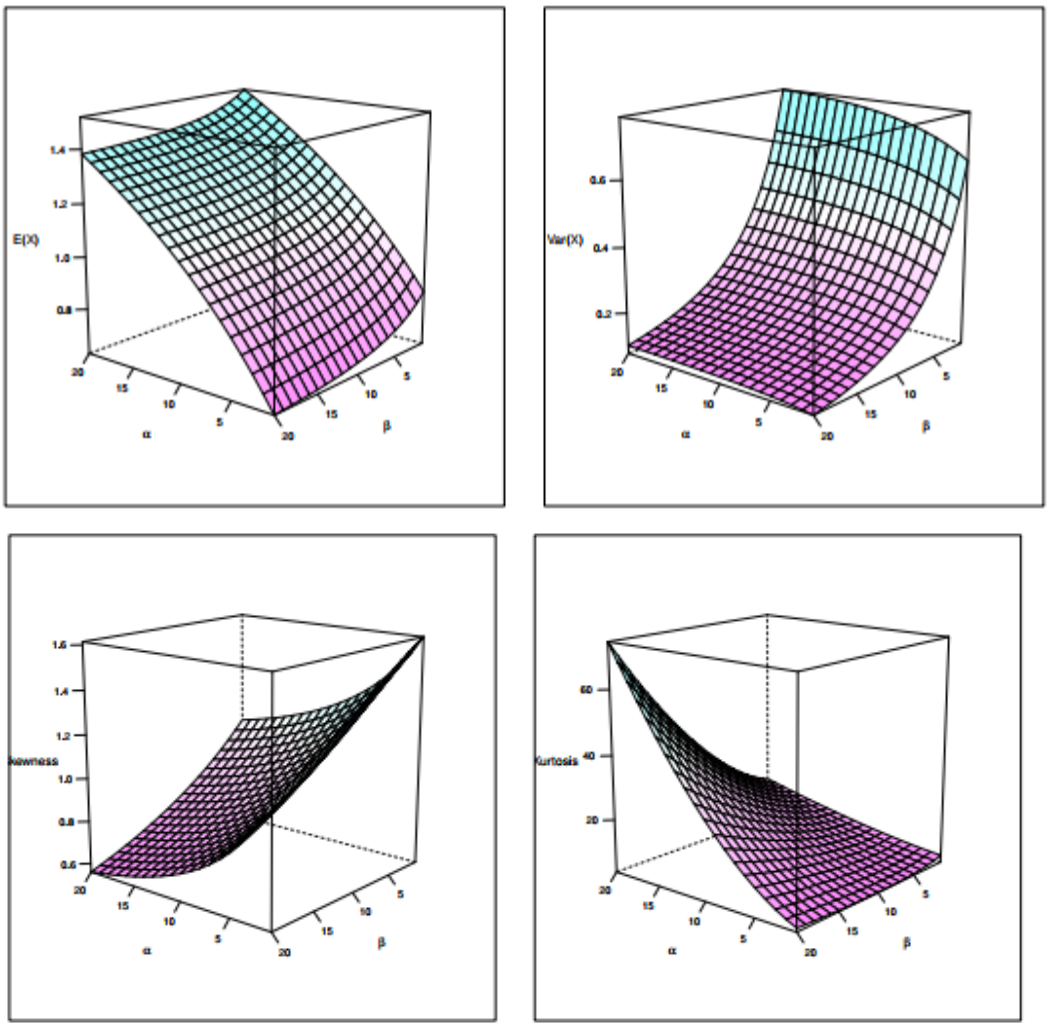

Figure 2: The plots of the expectation (top left), variance (top right), skewness (bottom left) and kurtosis (bottom right) for the GOLLX distribution using selected values of α and β for λ = 2.

3. KRIs

3.1 VaR indicator

Risk exposure is an inherent event for any insurance firm. Many actuaries developed a variety of risk indicators to measure risk exposure as a result. The VaR indicator determines the risk of a potential loss for the insurance company with a certain probability and calculates the amount that a group of investments might lose. An increasing used benchmark risk metric for determining risk exposure is this actuarial indicator. The VaR often determines how much capital is required, given a specific probability, to ensure that the firm won't officially go out of business. The chosen confidence level is arbitrary. As a result, a significant VaR amount may be considered for various levels of confidence. It can be a high percentage like 99.95% or higher for the entire company. These various percentages can represent the inter-unit or inter-risk type diversification that exists. The quantile function is generally used to find representations in terms of lookup tables for key percentiles. For $\alpha = \beta$. The algorithm is based on generating random data from the Lindley distribution mixturing the exponential and gamma distributions.

Algorithm 1:

1) Generate $U_{\xi}|_{[\xi=1,\ldots,n]} \sim$ Uniform$(0,1)$;
2) Generate $Z_{\xi}|_{[\xi=1,\ldots,n]} \sim$ Exponential(λ);
3) Generate $P_{\xi}|_{[\xi=1,\ldots,n]} \sim$ Gamma$(3,\lambda)$;

4) If $\frac{U_{\xi}^{\frac{1}{\alpha}}}{U_{\xi}^{\frac{1}{\alpha}}+(1-U_{\xi})^{\frac{1}{\alpha}}} \leq \frac{\lambda}{\lambda+1}$ set $X_{\xi} = Z_{\xi}$, $X_{\xi} = P_{\xi}|_{[\xi=1,\dots,n]}$.

Otherwise, if $u \sim U(0,1)$ the solution of eqution $F(\boldsymbol{x}) = u$ has CDF (cdfF).

Definition 1: *The VaR of* X at the $100q\%$ *level, say VaR* (X) *or* $\Delta_X(\rho)$ *, is the* $100q\%$ *quantile (or percentile (* Q_X *)) of the distribution of* X .

Then, based on Definition 1 for the GOLLX distribution, we can simply write

$$Pr(X > Q_X) = \begin{cases} 0.1\%|_{\rho=99.9\%} \\ 1\%|_{\rho=99\%} \\ \vdots \end{cases}, \tag{5}$$

where Q_X represents the numerical suotion of *Algorithm 1 (*see Wirch (1999)).

3.2 TVaR indicator

Definition 2: *Suppose that* X *denote a loss random variable. The TVaR* of X *at the* $100q\%$ *confidence level is the expected loss given that the loss exceeds the* $100q\%$ *of the distribution of* X , namely

$$\text{TVaR}(X) = \text{E}\big(X|_{[X>\Delta_X(\rho)]}\big) = \frac{1}{1-F_{\underline{V}}(\Delta_X(\rho))}\int_{\Delta_X(\rho)}^{\infty} \boldsymbol{x}\, f_{\underline{V}}(\boldsymbol{x})d\boldsymbol{x} = \frac{1}{\overline{\rho}}\int_{\Delta_X(\rho)}^{\infty} \boldsymbol{x}\, f_{\underline{V}}(\boldsymbol{x})d\boldsymbol{x}.$$

Let

$$\int_{\Delta_X(\rho)}^{\infty} \boldsymbol{x}^{\zeta_1}\,(0.5\lambda\boldsymbol{x}^2+1)[1-\mathcal{U}(\boldsymbol{x};\lambda)]^{\zeta_2}\frac{d\boldsymbol{x}}{exp(\zeta_3\boldsymbol{x})} = B(\zeta_1,\zeta_2,\zeta_3;\Delta_X(\rho),\lambda),$$

then,

$$B(\zeta_1,\zeta_2,\zeta_3;\Delta_X(\rho),\lambda) = \sum_{\xi=0}^{\infty}\sum_{(\xi_1,\xi_2)\in A} v_{\xi,\xi_1,\xi_2}\left\{\begin{matrix} \frac{1}{(\lambda\xi+\zeta_3)^{p^*+1}}\Gamma(p^*+1,\Delta_X(\rho)(\lambda\xi+\zeta_3)) \\ +\frac{0.5\eta}{(\lambda\xi+\zeta_3)^{p^*+3}}\Gamma(p^*+3,\Delta_X(\rho)(\lambda\xi+\zeta_3)) \end{matrix}\right\},$$

where $\Gamma(v,\mathcal{y}) = \int_{\mathcal{y}}^{\infty} e^{-t}\,t^{v-1}dt$ represent the lower incomplete gamma function and $\zeta_1 > 0, \zeta_2 \geq 1, \zeta_3 \geq 0$ are real numbers. Then,

$$\text{TVaR}(X) = C_{\lambda,\overline{\rho},\Delta_X(\rho)}\sum_{\varsigma,l=0}^{\infty}\sum_{\kappa=0}^{\varsigma}\sum_{\hbar=0}^{\varsigma-\kappa} q^* w_{\varsigma,\kappa,l,\hbar}B(1,q^*-1,\lambda;\Delta_X(\rho),\lambda), \tag{6}$$

where

$$C_{\lambda,\overline{\rho},\Delta_X(\rho)} = \frac{\lambda^2}{(\lambda+1)\overline{\rho}F(\Delta_X(\rho))}.$$

Thus, the quantity TVaR (X) can be expressed as an average of all VaR values above at the confidence level ρ , which provides more information about the tail of the GOLLX distribution. Further, it can also be expressed as

$$\text{TVaR}(X|_{\overline{\rho}}) = \text{VaR}(X|_{\overline{\rho}}) + m\big(X|_{\overline{\rho}}\big),$$

where $m\big(X|_{\overline{\rho}}\big)$ is the mean excess loss function evaluated at the $100q\%^{th}$ quantile. So, TVaR $(X|_{\overline{\rho}})$ is larger than its corresponding VaR $(X|_{\overline{\rho}})$ by the amount of average excess of all losses that exceed the EL $(X|_{\overline{\rho}})$ value of VaR $(X|_{\overline{\rho}})$. The VaR $(X|_{\overline{\rho}})$ has been independently developed and is also known as the conditional tail expectation in the insurance literature (see Wirch (1999); Tasche (2002); Acerbi and Tasche (2002)).

3.3 TV indicator

According to Tasche (2002); Acerbi and Tasche (2002), it has also been referred to as the expected shortfall (ExSh) or the tail conditional expectation (TCE). The loss's departure from the average is determined along a tail by the TV risk indicator, which Furman and Landsman (2006) established. Furman and Landsman (2006) also created explicit formulations for the TV risk indicator under the multivariate normal distribution.

Definition 3: *Suppose that* X *denote a loss random variable. The TV risk indicator (TVq(* X *)) can be expressed as*

$$\text{TV}(X|_{\overline{\rho}}) = E\big(X^2|X > \Delta_X(\rho)\big) - \big[\text{TVaR}(X|_{\overline{\rho}})\big]^2, \tag{7}$$

where TVaR (X) is defiend in (TVaR) and

$$E\left(X^2|X>\Delta_X(\rho)\right)=\frac{1}{1-F_{\underline{V}}\left(\Delta_X(\rho)\right)}\int_{\Delta_X(\rho)}^{\infty}\boldsymbol{x}^2\,f_{\underline{V}}(\boldsymbol{x})d\boldsymbol{x}=\frac{1}{\overline{\rho}}\int_{\Delta_X(\rho)}^{\infty}\boldsymbol{x}^2\,f_{\underline{V}}(\boldsymbol{x})d\boldsymbol{x},$$

then,

$$E\left(X^2|X>\Delta_X(\rho)\right)=\frac{\lambda^2}{(\lambda+1)(\overline{\rho})F(\Delta_X(\rho))}\sum_{\varsigma,l=0}^{\infty}\sum_{\kappa=0}^{\varsigma}\sum_{\hbar=0}^{\varsigma-\kappa}q^*\,w_{\varsigma,\kappa,l,\hbar}B(2,q^*-1,\lambda;\Delta_X(\rho),\lambda).$$

Finally, the TVq(X) can be expressed as

$$\mathrm{TV}(X|_{\overline{\rho}})=C_{\lambda,\overline{\rho},\Delta_X(\rho)}\left\{\begin{array}{l}\displaystyle\sum_{\varsigma,l=0}^{\infty}\sum_{\kappa=0}^{\varsigma}\sum_{\hbar=0}^{\varsigma-\kappa}q^*w_{\varsigma,\kappa,l,\hbar}\,B(2,q^*-1,\lambda;\Delta_X(\rho),\lambda)\\ -C_{\lambda,\overline{\rho},\Delta_X(\rho)}\left[\displaystyle\sum_{\varsigma,l=0}^{\infty}\sum_{\kappa=0}^{\varsigma}\sum_{\hbar=0}^{\varsigma-\kappa}q^*\,w_{\varsigma,\kappa,l,\hbar}B(1,q^*-1,\lambda;\Delta_X(\rho),\lambda)\right]^2\end{array}\right\}. \tag{8}$$

The last formula and other formulas in this paper can be dealt with and its mathematical complexities can be overcome numerically through some statistical programs and packages like "R" and "MATHCAD", among others. This is what has already been implemented to calculate all the previously presented risk measures and other calculations in the aspect of estimation, simulation, applications, etc. And the growing development in statistical assertions has made this task easier for us and made it easy to accomplish. We do not claim that these series are convergent series, but we confirm that we have been able to find suitable approximate numerical values for all these quantities, and this is what helped complete the numerical results and accomplish the related practical applications.

3.4 TMV risk indicator

As a metric for the best portfolio choice, Landsman (2010). developed the TMV risk indicator, which is based on the TCE risk indicator and the TV risk indicator.

Definition 4: *Suppose that X denote a loss random variable. The TMV risk indicator can then be expressed as*

$$\mathrm{TMV}(X|_{\overline{\rho}})=\mathrm{TVaR}(X|_{\overline{\rho}})+\pi\mathrm{TV}(X|_{\overline{\rho}})|_{0<\pi<1}. \tag{9}$$

Then, for any loss random variable, TMV $(X|_{\overline{\rho}})>$ TV $(X|_{\overline{\rho}})$ and, for $\pi=0$, TMV $(X|_{\overline{\rho}})=$ TVaR $(X|_{\overline{\rho}})$, for $\pi=1$, TMV $(X|_{\overline{\rho}})=$ TVaR $(X|_{\overline{\rho}})+$ TV $(X|_{\overline{\rho}})$ and when $\pi\to 0$, TMV $(X|_{\overline{\rho}})\to$ TVaR $(X|_{\overline{\rho}})$.

3.5 The PORT-VaR methodology

According to Alizadeh et al. (2023, 2024 and 2015), Aljadani et al. (2024) and Das et al. (25), the PORT-VaR approach is employed alongside the traditional VaR estimate to rigorously detect and analyze extreme financial events in insurance data. While conventional VaR methods provide a static quantile-based threshold for loss estimation, PORT-VaR introduces a dynamic perspective by focusing on the distribution of exceedances above randomly selected thresholds. This allows for greater sensitivity in identifying clusters of extreme values that may otherwise remain undetected. The two methods are contrasted to evaluate their effectiveness in capturing tail risk, particularly in non-normal, skewed distributions often observed in insurance and reinsurance data. PORT-VaR's flexibility enables it to adapt to the irregularities of financial extremes, offering a richer understanding of the risk structure. When applied to insurance claims, it helps isolate the most severe loss events, while for reinsurance revenues, it exposes windfall peaks beyond standard expectations. This comparative analysis offers a nuanced view of financial extremes and highlights the importance of choosing appropriate models for tail risk detection in the insurance sector.

4. Applications and modeling

From complete samples, we derive the maximum likelihood estimates (MLEs) of the GOLLX distribution's parameters. Using two real data sets, we demonstrate in this section how well the GOLLX distribution fits. We compared the models we fitted to see how well the GOLLX distribution fits with actual data: Lindley distribution, power Lindley distribution, generalized Lindley, Weibull distribution, exponential distribution, gamma distribution, and odd log-logistic Distribution by Lindley Odd log-logistic Weibull distribution, the X-Gamma distribution, and OLLL Odd Logistic Logistic X-Gamma Distribution, or OLLW The new odd log-logistic X-Gamma distribution is called OLL-XGamma. NOLL-XGamma. The maximum likelihood estimates (MLEs), the standard errors are presented for each dataset. The Akaike Information Criterion (AIC), Bayesian Information Criterion (BIC), Cramer

Von Mises (W^*) and Anderson-Darling statistics (A^*) are used for comparing the competitive models. For comparison's sake, we also considered the Kolmogorov-Smirnov (K-S) statistic, its accompanying p-value, and the minimal value of the minus log-likelihood function ($-l$). Generally, the smaller values of A^*, W^*, p-value, AIC, BIC and $-l$ the better fit to a data set. The programme R was used to do all the computations.

The first set of information consists of the Wheaton River's near-Carcross, Yukon Territory, Canada, exceedances of flood peaks (measured in m3/s). The information consists of 72 exceedances with one decimal place over the years 1958 to 1984. (see Table 1). The MLEs (standard errors in parentheses) for the first data set are shown in Table 2. The goodness-of-fit test statistics for the initial data set are shown in Table 3. The second data set is related to failure time of 40 devices given by Murthy et al. (2019) (see Table 4). Table 5 gives the MLEs (standard errors in the parentheses) for the failure times data set (second data set). Table 6 lists the goodness-of-fit test statistics for the failure times data set (second data set). The third data, a list of complete extreme natured skewed to right data, discussed by Murthy et al. (2019), represents the failure times of 20 components (see Table 7). Table 8 gives the MLEs (standard errors in the parentheses) for third data set. Table 9 lists the goodness-of-fit test statistics for the failure times data set of 20 components (third data set). The fourth data set given below represents the failure times of 50 components. For previous study on this data set see Merovci et al. (2020) (see Table 10). Table 11 gives the MLEs (standard errors in the parentheses) for fourth data set. Table 12 lists the goodness-of-fit test statistics for the failure times data set of 50 components (fourth data set).
The four actual data sets are evaluated first. In general, the analysis of real data can be done analytically, visually, or by combining the two approaches. We address both numerical methodologies and many graphical tools, such as the skewness-kurtosis plot, to assess the initial fits of theoretical distributions like as the normal, uniform, exponential, logistic, beta, lognormal, and Weibull (or the Cullen and Frey plot). For higher accuracy, plotting and bootstrapping are also used. Cullen and Frey's figure only compares distributions in the space of, despite being a fantastic depiction (squared skewness, kurtosis). To analyze the initial form of the empirical HRF, the "total time in test (TTT)" plot, the "box plot," the "nonparametric Kernel density estimation (NKDE)" approach, and the determination of the extreme observations are all considered. Figure 3 provides the TTT plots for the four data sets respectively. Figure 4 shows the box plots for the four data sets respectively. Figure 5 presents the Q-Q plots for the four data sets respectively. Figure 6 presents the NKDE plots for the four data sets respectively. Figure 7 presents the Cullen and Frey plots for the four data sets respectively. The 1st plots for the exceedances of flood peaks data, the top right plots for the failure time of 40 devices data, the bottom left plots for the failure times of 20 components data and the bottom right plots for the failure times of 50 components data. Due to Figure 3, it is noted that the HRF of the exceedances of flood peaks data is "monotonically increasing HRF", the HRF of the failure time of 40 devices data is "monotonically increasing HRF", the HRF of the failure times of 20 components data is "increasing-decreasing-increasing" shape and the HRF of the failure times of 50 components data is "monotonically decreasing" shape. Based on Figure 4, it is noted that the exceedances of flood peaks data have some extreme values, the failure time of 40 devices data has no extreme values, the failure times of 20 components data has no extreme values and the HRF of the failure times of 50 components data has some extreme values. Due Figure 5, it is noted that the exceedances of flood peaks data have two extreme values, the failure time of 40 devices data has no extreme values, the failure times of 20 components data has no extreme values and the HRF of the failure times of 50 components data has two extreme values. Based on Figure 6, it is noted that the exceedances of flood peaks data is asymmetric density with bimodal shape and heavy right tail, the failure time of 40 devices data is asymmetric density with bimodal shape and right tail, the failure times of 20 components data is asymmetric density with bimodal shape and right tail and the HRF of the failure times of 50 components data is asymmetric density with bimodal shape and heavy right tail. Based on Figure 7, it is seen that all data does not follow any of the standard distributions including the normal, exponential, uniform, logistic, lognormal, beta, and Weibull. Figure 8 gives the fitted PDFs (the first and the second panels) and fitted CDFs (the third and the fourth panels) for all competitive distributions for first data set. Figure 9 gives the fitted PDFs (the first and the second panels) and fitted CDFs (the third and the fourth panels) for all competitive distributions for second data set. Figure 10 gives the fitted PDFs (the first and the second panels) and fitted CDFs (the third and the fourth panels) for all competitive distributions for third data set. Figure 11 gives the fitted PDFs (the first and the second panels) and fitted CDFs (the third and the fourth panels) for all competitive distributions for fourth data set. Due to Figure 8, Figure 9, Figure 10 and Figure 11 the proposed model provides adequate fits to the empirical data.

Based on Table 3, it is noted that the GOLLX model has proven its superiority and applicability in the field of statistical modeling of the exceedances of flood peaks data, and the results of the GOLLX distribution are the best ever compared to other competing distributions, where $A^* = 0.0441$, $W^* = 0.2780$, p-value=0.6406, $AIC = 502.5833$, BIC =509.4133 and $-l = 248.2917$. Based on Table 6, it is noted that the GOLLX model has proven its superiority and applicability

in the field of statistical modeling of the failure times data, and the results of the GOLLX distribution are the best ever compared to other competing distributions, where $A^* = 0.0554$, $W^* = 0.4338$, p-value= 0.8421, $AIC = 57.1990$, $BIC = 62.26565$ and $-l = 25.5995$. Based on Table 9, it is noted that the GOLLX model has proven its superiority and applicability in the field of statistical modeling of the failure times of 20 components data, and the results of the GOLLX distribution are the best ever compared to other competing distributions, where $A^* = 0.0439$, $W^* = 0.3049$, p-value= 0.9322, $AIC = 172.3996$, $BIC = 175.3868$ and $-l = 83.1998$. Based on Table 12, it is noted that the GOLLX model has proven its superiority and applicability in the field of statistical modeling of the failure times of 50 components data, and the results of the GOLLX distribution are the best ever compared to other competing distributions, where $A^* = 0.0541$, $W^* = 0.4351$, p-value= 0.9752, $AIC = 198.9925$, $BIC = 204.7286$ and $-l = 96.49627$. The p-value, used in null-hypothesis significance statistical testing, represents the likelihood that the test findings will be at least as severe as the result actually observed, assuming that the null hypothesis is true. A very low p-value indicates that the null hypothesis would not accept the extreme observed event. Generally, the p-values are 0.6406, 0.8421, 0.9322 and 0.9752 for the four real data sets respectively. Table 13 gives the LR test and its related results for the four real data sets respectively.

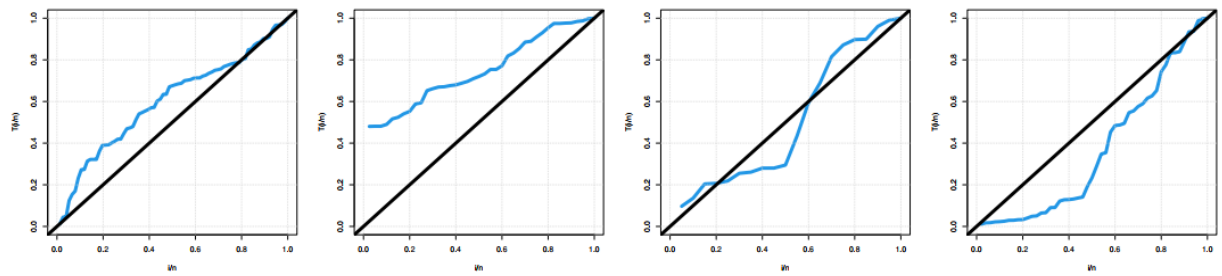

Figure 3: The TTT plots.

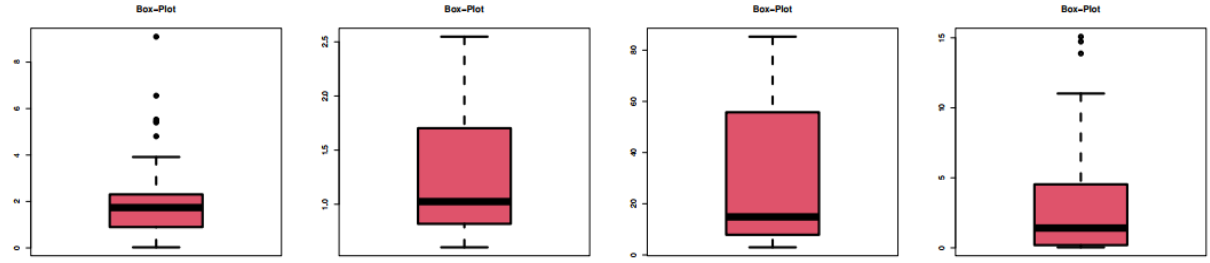

Figure 4: Box plots.

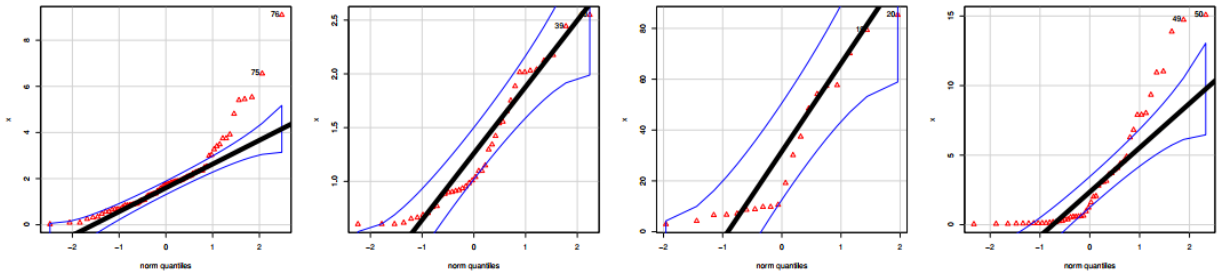

Figure 5: Q-Q plots.

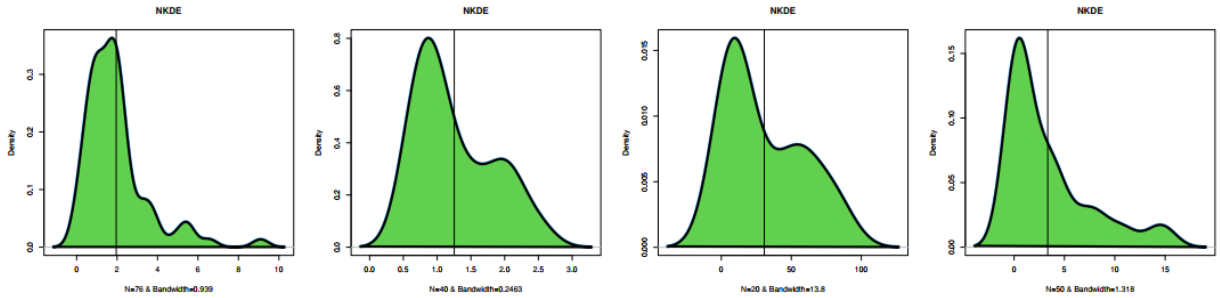

Figure 6: NKDE plots.

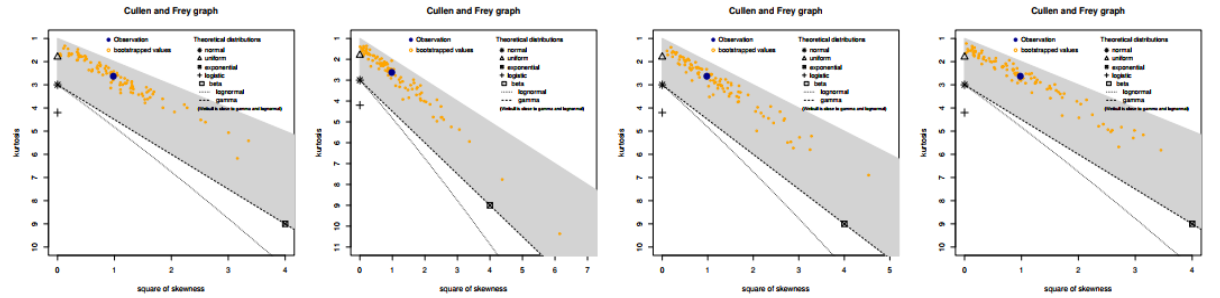

Figure 7: Cullen and Frey plots.

Table1: First data set.

1.70	2.20	14.4	1.10	0.40	20.6	5.30	0.70	1.90	13.0	12.0	9.30	1.40
18.7	8.50	25.5	11.6	14.1	22.1	1.10	2.50	14.4	1.70	37.6	0.60	2.20
39.0	0.30	15.0	11.0	7.30	22.9	1.70	0.10	1.10	0.60	9.00	1.70	7.00
20.1	0.40	2.80	14.1	9.90	10.4	10.7	30.0	3.60	5.60	30.8	13.3	4.20
25.5	3.40	11.9	21.5	27.6	36.4	2.70	64.0	1.50	2.50	27.4	1.00	27.1
			20.2	16.8	5.30	9.70	27.5	2.50	27.0			

Table 2: Estimation results for the first data.

Model	$\hat{\lambda}$ (SE)	$\hat{\alpha}$ (SE)	$\hat{\beta}$ (SE)
Exponential (λ)	0.0819 (0.0096)	--	--
Weibull (α, λ)	11.634 (1.6022)	0.9011 (0.0855)	--
Gamma (α, λ)	0.8377 (0.1209)	0.0686 (0.0132)	--
GE (α, λ)	0.0724 (0.011)	0.8281 (0.1230)	--
Lindley (λ)	0.1529 (0.0127)	--	--
GL (α, λ)	0.1042 (0.0149)	0.5087 (0.0766)	--
PL (α, λ)	0.3384 (0.0558)	0.7001 (0.0569)	--
EPL (α, β, λ)	0.3002 (0.2786)	0.7298 (0.234)	0.9156 (0.5944)
OLLL (α, λ)	0.1836 (0.0220)	0.6122 (0.0660)	--
OLLPL (α, β, λ)	0.1549 (0.0910)	1.0736 (0.2434)	0.5577 (0.1772)
OLLW (α, β, λ)	11.278 (1.5062)	0.5915 (0.1498)	1.3804 (0.2848)
XGamma (λ)	0.2044 (0.015)	--	--
OLLX (α, λ)	0.2391 (0.0254)	0.6120 (0.0658)	--
NOLLX (α, β, λ)	0.6669 (0.0026)	1.2038 (0.1848)	0.1538 (0.0204)
GOLLX (α, β, λ)	0.6387 (0.0047)	5.5615 (0.0156)	0.1988 (0.0193)

Table 3: Fitting results for the first data.

Model	W^*	A^*	p-value	AIC	BIC	$-l$
Exponential (λ)	0.1305	0.7523	0.1088	506.2561	508.5326	252.128
Weibull (α, λ)	0.1379	0.7854	0.4025	506.9973	511.5506	251.4986
Gamma (α, λ)	0.1563	1.0714	2.2e-16	506.6887	511.2421	251.3444
GE (α, λ)	0.1285	0.7420	0.4471	506.5871	511.1404	251.2936
Lindley (λ)	0.1391	0.8521	0.001	530.4231	532.7001	264.211
GL (α, λ)	0.1322	0.8222	0.276	509.3492	513.9022	252.674
PL (α, λ)	0.1231	0.7662	0.405	508.4431	512.9961	252.103
EPL (α, β, λ)	0.1472	0.8541	0.395	510.4252	517.2552	252.212
OLLL (α, λ)	0.1001	0.6213	0.501	506.0291	510.5821	251.015
OLLPL (α, β, λ)	0.1330	0.8623	<0.001	507.9373	514.7673	250.9687
OLLW (α, β, λ)	0.1525	0.9890	0.0007	534.9293	537.2060	266.4647
XGamma (λ)	0.0744	0.4737	0.5158	505.8522	512.6822	249.9261
OLLX (α, λ)	0.1236	0.8126	0.2476	510.1478	514.7011	253.0739
NOLLX (α, β, λ)	0.0953	0.5051	0.1108	505.6432	512.4732	249.8216
GOLLX (α, β, λ)	0.0441	0.2780	0.6406	502.5833	509.4133	248.2917

Table 4: Second data set.

0.602	0.603	0.603	0.615	0.652	0.663	0.688	0.705	0.761	0.770
0.868	0.884	0.898	0.901	0.911	0.918	0.935	0.953	0.983	1.009
1.040	1.097	1.097	1.148	1.296	1.343	1.422	1.540	1.555	1.653
1.752	1.885	2.015	2.015	2.030	2.040	2.123	2.175	2.443	2.548

Table 5: Estimation results for the second data.

Model	$\hat{\lambda}$ (SE)	$\hat{\alpha}$ (SE)	$\hat{\beta}$ (SE)
Exponential (λ)	0.7978 (49.036)	--	--
Weibull (α, λ)	1.4214 (0.0995)	2.3948 (0.2884)	--
Gamma (α, λ)	5.2912 (1.1477)	4.2214 (0.9606)	--
GE (α, λ)	2.2484 (0.3361)	8.7053 (3.0073)	--
Lindley (λ)	1.1662 (0.1410)	--	--
GL (α, λ)	2.6156 (0.3491)	7.2935 (2.5363)	--
PL (α, λ)	0.8044 (0.1232)	2.0437 (0.2277)	
EPL (α, β, λ)	7.0753 (1.9847)	0.3935 (0.1196)	546.09 (1057.61)
OLLL (α, λ)	0.9969 (0.0615)	2.3152 (0.2984)	--
OLLPL (α, β, λ)	1.1096 (0.0105)	0.0885 (0.0879)	27.543 (42.7398)
OLLW (α, β, λ)	18.846 (29.051)	20.855 (11.695)	0.1297 (0.0708)
XGamma (λ)	1.5082 (0.1721)	--	--
OLLX (α, λ)	1.2389 (0.0672)	2.5823 (0.3338)	--
NOLLX (α, β, λ)	3.9132 (1.4205)	15.523 (13.673)	0.3776 (0.2080)
GOLLX (α, β, λ)	7.4010 (1.7777)	308.37 (400.97)	0.3166 (0.1021)

Table 6: Fitting results for the second data

Model	W^*	A^*	p-value	AIC	BIC	$-l$
Exponential (λ)	0.1656	1.0054	<0.001	100.073	101.7625	49.0367
Weibull (α, λ)	0.2269	1.3197	0.2634	67.1666	68.38797	31.5833
Gamma (α, λ)	0.1699	1.0277	<0.001	63.6594	67.03721	29.8297
GE (α, λ)	0.1355	0.8585	0.6813	62.3528	65.73065	29.1764
Lindley (λ)	0.1757	1.0574	<0.001	93.5442	95.23313	45.7721
GL (α, λ)	0.1426	0.8935	0.6353	62.7239	66.10172	29.3619
PL (α, λ)	0.2408	1.3958	0.2769	68.4038	71.78163	32.2019
EPL (α, β, λ)	0.0920	0.6611	0.8071	62.6354	67.70209	28.3177
OLLL (α, λ)	0.1846	1.1252	0.6368	66.5583	69.93611	31.2791
OLLPL (α, β, λ)	0.1280	0.8207	<0.001	67.4507	72.51735	30.7253
OLLW (α, β, λ)	0.1880	1.1172	<0.001	99.3256	101.0145	48.6628

XGamma (λ)	0.1463	0.9454	0.7812	67.4612	72.52785	30.7306
OLLX (α, λ)	0.1934	1.1668	0.5767	66.7475	70.12532	31.3737
NOLLX (α, β, λ)	0.0875	0.6888	0.5691	64.2617	69.32842	29.1308
GOLLX (α, β, λ)	0.0554	0.4338	0.8421	57.1990	62.26565	25.5995

Table 7: Third data set.

2.968	4.229	6.560	6.662	7.110	8.608	8.851	9.763	9.773	10.578
19.136	30.112	37.386	48.442	54.145	57.337	57.637	70.175	79.333	85.283

Table 8: Estimation results for the third data.

Model	$\hat{\lambda}$ (SE)	$\hat{\alpha}$ (SE)	$\hat{\beta}$ (SE)
Exponential (λ)	0.0326 (0.0072)	--	--
Weibull (α, λ)	31.619 (6.9578)	1.0753 (0.1914)	--
Gamma (α, λ)	1.1439 (0.3219)	0.0372 (0.0130)	--
GE (α, λ)	0.0355 (0.0100)	1.1482 (0.3444)	--
Lindley (λ)	0.0631 (0.0099)	--	--
GL (α, λ)	0.0476 (0.0123)	0.6017 (0.1776)	--
PL (α, λ)	0.1438 (0.0615)	0.7713 (0.1145)	--
EPL (α, β, λ)	2.3754 (3.1450)	0.2506 (0.2034)	37.2465 (136.3805)
OLLL (α, λ)	0.0708 (0.0143)	0.6895 (0.1320)	--
OLLPL (α, β, λ)	0.0025 (0.0011)	1.9451 (0.1276)	0.28144 (0.06742)
OLLW (α, β, λ)	37.796 (7.7066)	0.3207 (0.1719)	2.95583 (1.35545)
XGamma (λ)	0.0894 (0.0121)	--	--
OLLX (α, λ)	0.1044 (0.0192)	0.5965 (0.1172)	--
NOLLX (α, β, λ)	0.4704 (0.0072)	4.0062 (1.1416)	0.0783 (0.01965)
GOLLX (α, β, λ)	0.4558 (0.0135)	44.757 (0.1074)	0.0898 (0.01656)

Table 9: Fitting results for the third data

Model	W^*	A^*	p-value	AIC	BIC	$-l$
Exponential (λ)	0.1624	0.9269	0.3072	178.9763	179.9721	88.4881
Weibull (α, λ)	0.1633	0.9322	0.1872	180.8145	182.8062	88.4072
Gamma (α, λ)	0.3401	2.1121	<0.001	180.7582	182.7491	88.3791
GE (α, λ)	0.1625	0.9274	0.1828	180.7681	182.7592	88.3839
Lindley (λ)	0.1684	0.9648	0.0168	182.6236	183.6192	90.3117
GL (α, λ)	0.1682	0.9639	0.1621	181.3835	183.3753	88.6917
PL (α, λ)	0.1649	0.9432	0.2013	181.1429	183.1344	88.5714
EPL (α, β, λ)	0.1402	0.8048	0.4017	182.2363	185.2235	88.1181
OLLL (α, λ)	0.1571	0.8936	0.2255	180.0585	182.0499	88.0292
OLLPL (α, β, λ)	0.1884	1.0923	0.0162	179.0443	182.0315	86.5221
OLLW (α, β, λ)	0.1927	1.1207	0.0035	189.4791	190.4748	93.7395
XGamma (λ)	0.1383	0.8122	0.0904	180.3212	183.3084	87.1605
OLLX (α, λ)	0.1758	1.0144	0.1905	182.4126	184.4041	89.2063
NOLLX (α, β, λ)	0.0484	0.3450	0.7199	173.3923	176.3772	83.6950
GOLLX (α, β, λ)	0.0439	0.3049	0.9322	172.3996	175.3868	83.1998

Table 10: Fourth data set.

0.036	0.058	0.061	0.074	0.078	0.086	0.102	0.103	0.114	0.116
0.148	0.183	0.192	0.254	0.262	0.379	0.381	0.538	0.570	0.574
0.590	0.618	0.645	0.961	1.228	1.600	2.006	2.054	2.804	3.058
3.076	3.147	3.625	3.704	3.931	4.073	4.393	4.534	4.893	6.274
6.816	7.896	7.904	8.022	9.337	10.94	11.02	13.88	14.73	15.08

Table 11: Estimation results for the fourth data.

Model	$\hat{\lambda}$ (SE)	$\hat{\alpha}$ (SE)	$\hat{\beta}$ (SE)
Exponential (λ)	0.2991 (0.0423)	--	--
Weibull (α, λ)	2.5312 (0.5717)	0.6612 (0.0747)	--
Gamma (α, λ)	0.5454 (0.0907)	0.1631 (0.0413)	
GE (α, λ)	0.1941 (0.0431)	0.5369 (0.0901)	--
Lindley (λ)	0.4988 (0.0513)	--	--
GL (α, λ)	0.2965 (0.0541)	0.4112 (0.0711)	--
PL (α, λ)	0.9276 (0.1224)	0.5813 (0.0623)	--
EPL (α, β, λ)	1.4774 (1.1987)	0.429 (0.2545)	1.8308 (2.2588)
OLLL (α, λ)	0.6262 (0.0968)	0.5216 (0.0665)	--
OLLPL (α, β, λ)	0.7447 (0.2284)	0.8552 (0.2494)	0.6254 (0.2244)
OLLW (α, β, λ)	2.6514 (0.6030)	0.5267 (0.1766)	1.1408 (0.3271)
XGamma (λ)	0.6173 (0.0585)	--	--
OLLX (α, λ)	0.7413 (0.1028)	0.5582 (0.0711)	--
NOLLX (α, β, λ)	2.7791 (0.0039)	1.1906 (0.2029)	0.1042 (0.01760)
GOLLX (α, β, λ)	2.7795 (0.0040)	8.3478 (0.0357)	0.1288 (0.01514)

Table 12: Fitting results for the fourth data

Model	W^*	A^*	p-value	AIC	BIC	$-l$
Exponential (λ)	0.1503	0.9602	0.0004	222.6857	224.5977	110.3428
Weibull (α, λ)	0.1522	0.9543	0.3643	208.7286	212.5527	102.3643
Gamma (α, λ)	0.1893	1.2320	<0.001	208.8735	212.6975	102.4367
GE (α, λ)	0.1470	0.9418	0.2346	208.7449	212.5691	102.3725
Lindley (λ)	0.1721	1.1110	<0.001	242.3559	244.2679	120.178
GL (α, λ)	0.1714	1.1139	0.1255	211.9627	215.7868	103.9814
PL (α, λ)	0.1564	0.9829	0.3462	209.4877	213.3117	102.7438
EPL (α, β, λ)	0.1600	0.9954	0.4904	211.1786	216.9147	102.5893
OLLL (α, λ)	0.1405	0.9487	0.1451	208.5306	212.3547	102.2653
OLLPL (α, β, λ)	0.1697	1.0956	0.0150	210.2107	215.9468	102.1054
OLLW (α, β, λ)	0.1204	0.8183	0.1954	208.1783	213.9144	101.0892
XGamma (λ)	0.1590	1.0604	<0.001	233.9803	235.8923	115.9902
OLLX (α, λ)	0.1449	0.9939	0.1035	208.1222	211.9462	102.0611
NOLLX (α, β, λ)	0.0463	0.3487	0.9171	198.7472	204.4833	96.3736
GOLLX (α, β, λ)	0.0541	0.4351	0.9752	198.9925	204.7286	96.49627

Table 13: LR test and its related results.

Data and Models↓ Hypotheses→	Hypotheses	LR	p-value
The 1st data set			
NOLLX versus X-gamma	$H_0: \alpha = \beta = 1$	36.346	<0.001
NOLLX versus OLLX	$H_0: \alpha = 1$	9.5644	0.0012
NOLLX versus exponentiated XGamma	$H_0: \beta = 1$	11.968	0.0005
The 2nd data set			
NOLLX versus XGamma	$H_0: \alpha = \beta = 1$	46.12661	<0.001
NOLLX versus OLLX	$H_0: \alpha = 1$	11.54856	0.0006
NOLLX versus exponentiated XGamma	$H_0: \beta = 1$	8.141115	0.0043
The 3rd data set			
NOLLX versus X-Gamma	$H_0: \alpha = \beta = 1$	21.07938	<0.001
NOLLX versus OLLX	$H_0: \alpha = 1$	12.01295	0.0005
NOLLX versus exponentiated XGamma	$H_0: \beta = 1$	14.64287	0.0001
The 4th data set			

NOLLX versus XGmma	$H_0: \alpha = \beta = 1$	38.98778	<0.001
NOLLX versus OLLX	$H_0: \alpha = 1$	11.12962	0.0008
NOLLX versus exponentiated XGamma	$H_0: \beta = 1$	12.47517	0.0004

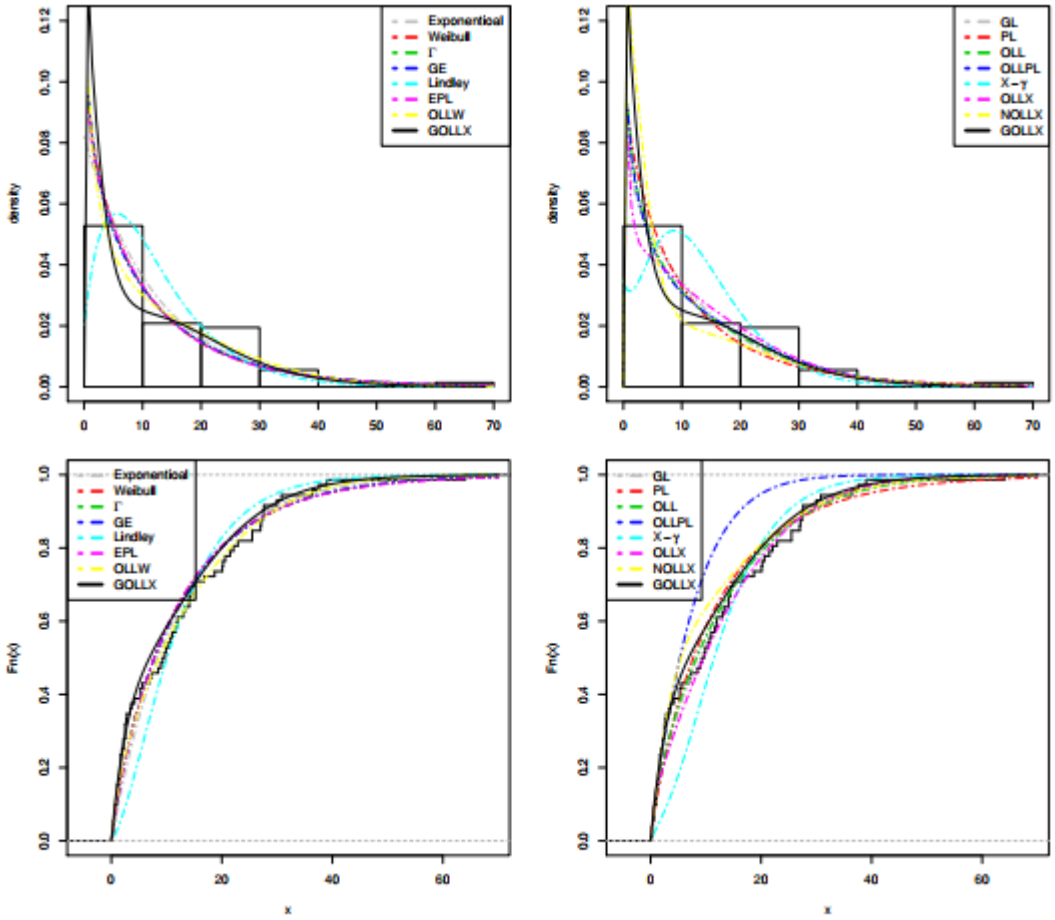

Figure 8: The fitted PDFs (the first and the second panels) and fitted CDFs (the third and the fourth panels) for all competitive distributions for first data set.

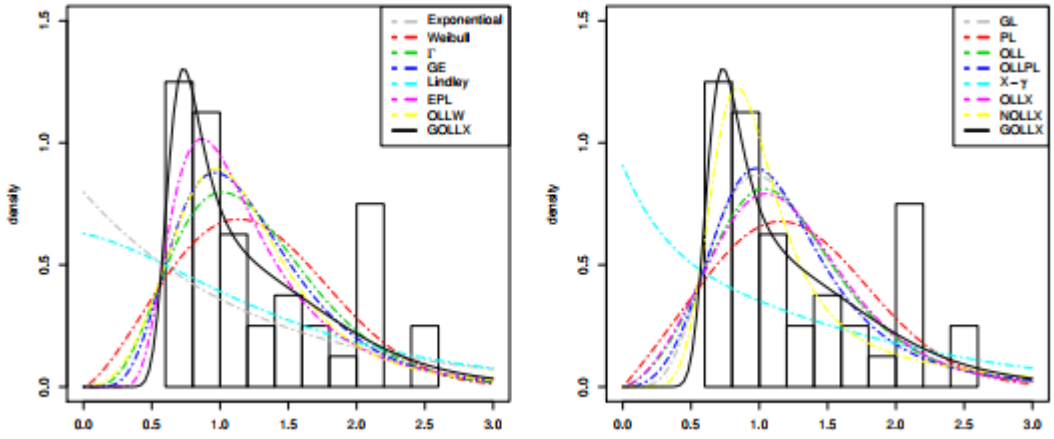

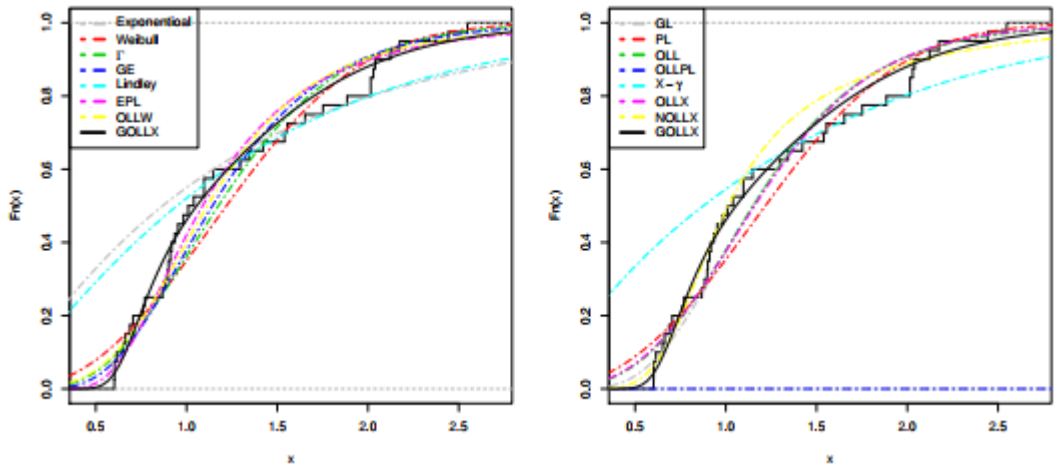

Figure 9: The fitted PDFs (the first and the second panels) and fitted CDFs (the third and the fourth panels) for all competitive distributions for second data set.

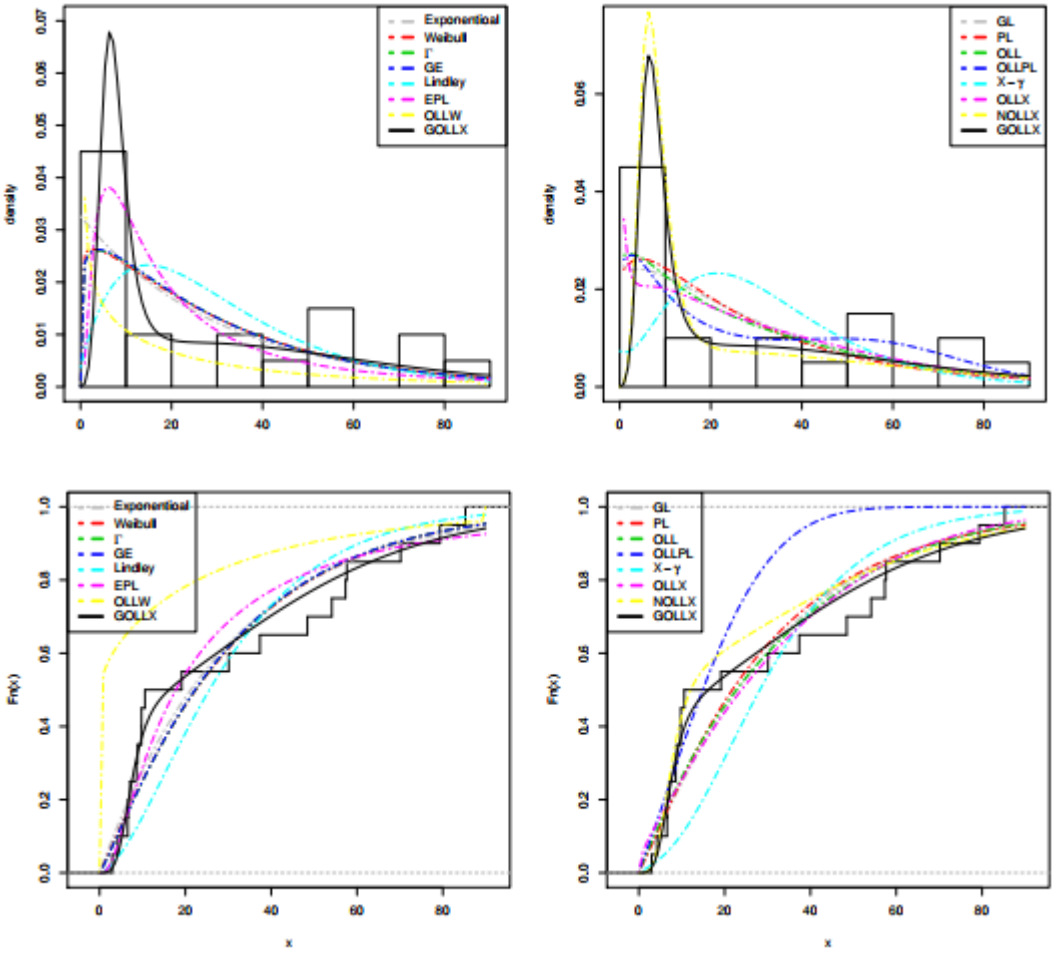

Figure 10: The fitted PDFs (the first and the second panels) and fitted CDFs (the third and the fourth panels) for all competitive distributions for third data set.

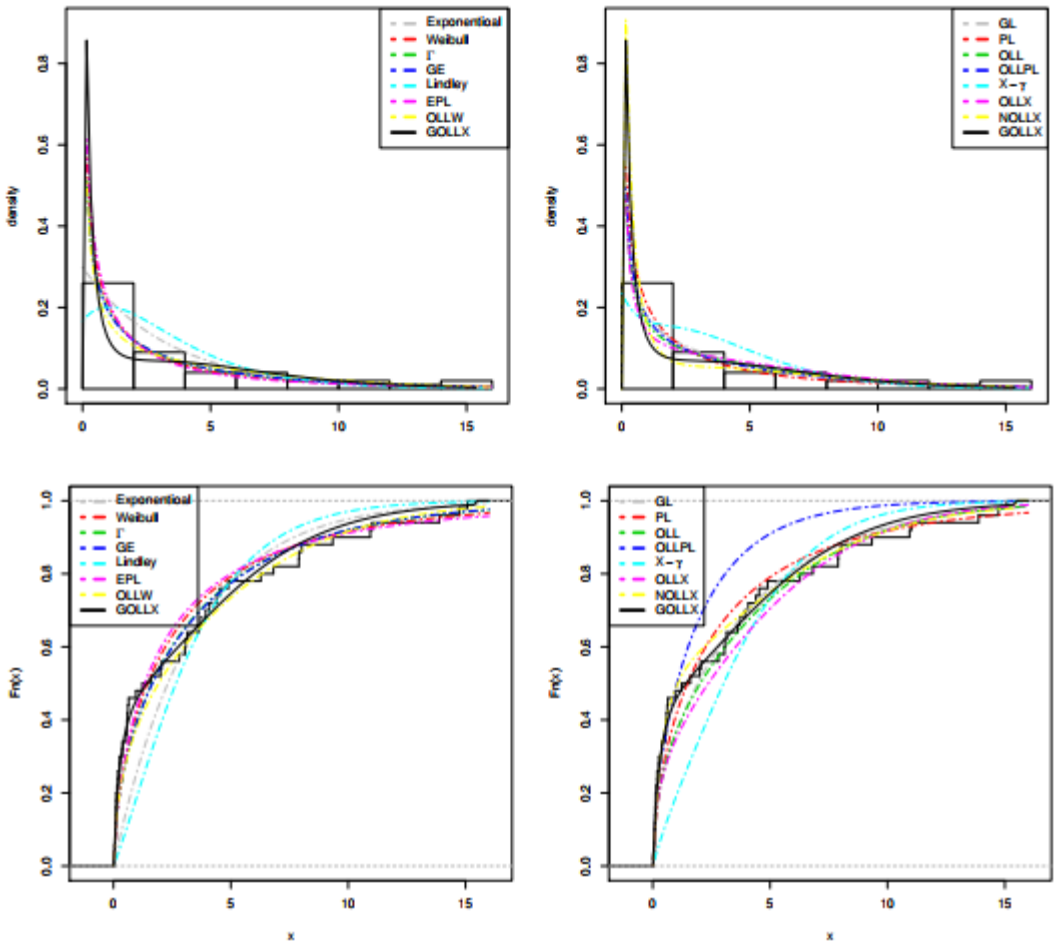

Figure 11: The fitted PDFs (the first and the second panels) and fitted CDFs (the third and the fourth panels) for all competitive distributions for fourth data set.

5. Risk analysis under the insurance claims and reinsurance revenues data sets

This section discusses the insurance claims and reinsurance firm revenue in the American insurance sector. In the historical insurance actual data, the temporal growth of claims over time for each relevant exposure (or origin) period is typically presented as a triangle. The exposure period may be thought of as the year the insurance policy was bought or the time frame in which the loss occurred. That the genesis time need not be annual is clear. For instance, origin periods could be monthly or quarterly. The term "claim age" or "claim lag" refers to the length of time that an origin period took to emerge. To representing uniform business lines, division levels, or dangers, data from various insurances is routinely integrated. In this article, we look at the insurance claims payment triangle using a U.K. Motor Non-Comprehensive account as a first real example. We pick the practical genesis period of 2007 to 2013 (see Charpentier (2024) and also (see Korkmaz et al. (2017, 2018), Khedr et al. (2023) and Ibrahim et al. (2023, 2025), Shrahili et al. (2021), Mohamed et al. (2022) and Mohamed et al. (2024) for more analysis). The claims data is presented in the insurance claims payment data frame in the same way that a database would typically store it. The first column contains the development year, the incremental payments, and the origin year, which spans from 2007 to 2013. It's vital to remember that a probability-based distribution was initially used to analyze this data on insurance claims.

The second example relates to data on reinsurance revenue, which is currently represented as a monthly time series of data. Fortunately, our data are current time series data with a start date of February 2015 and a finish date of April 2020, the data is available at *https://data.world/datasets/insurance*. The information on insurance claims and reinsurance revenues must be looked at first. Real data can be examined using numerical and graphical methods. We cover a variety of graphical approaches, such as the skewness-kurtosis plot (also known as the Cullen and Frey plot), for examining early fits of theoretical distributions such the normal, logistic, uniform, exponential, beta, lognormal,

and Weibull. For more accuracy, the bootstrapping results are used and plotted. Cullen and Frey's graphic only compares distributions in the space of the squared skewness, kurtosis, while being an excellent depiction of the properties of the distributions. Other graphical tools include the NKDE approach for examining the initial shape of the empirical hazard rate function, the box plot for identifying the extreme reinsurance revenues, and TTT plot for examining the initial shape of the empirical hazard rate function. Table 14 gives summary statistics for the insurance claims and reinsurance revenue data.

In this application, we discuss many graphical methods for analyzing early fits of theoretical distributions such the normal, logistic, uniform, exponential, beta, lognormal, and Weibull, such as the skewness-kurtosis plot (also known as the Cullen and Frey plot). The bootstrapping findings are applied and displayed for more accuracy. The picture by Cullen and Frey is a superb representation of the characteristics of the distributions, however it only compares distributions in the space of the squared skewness, kurtosis. Other graphical techniques include the TTT plot for assessing the initial form of the empirical hazard rate function, the "box plot" for finding the extreme reinsurance revenues, and the NKDE approach.

The Cullen and Frey plot for the data of the insurance claims is shown in Figure 12 (see right panel). The Cullen and Frey plot for the data of reinsurance revenues is shown in Figure 12 (see left panel). The NKDE plot for the data of the insurance claims is shown in Figure 13 (top left panel). Figure 13 (2nd plot) displays the Q-Q plot for the data of the insurance claims. The TTT plot for the data of the insurance claims data is shown in Figure 13 (the 3rd plot), and Figure 13 (the bottom right panel) displays a box plot of the data for insurance claims. The NKDE plot for the data of reinsurance revenues is shown in Figure 14 (top left figure). Figure 14 (2nd plot) displays the Q-Q plot for the data of the reinsurance revenues. The TTT plot for the data of the reinsurance revenues data is shown in Figure 14 (the 3rd plot), and Figure 14 (the bottom right panel) displays a box plot of the data for reinsurance revenues. Due to Figure 13 (top left figure), the insurance claims data are left skewed, where the skewness= -0.748278 and the kurtosis= 2.7884640 . No extreme observations are spotted based on Figure 13 (top right and bottom right plots) due to the insurance claims data. Further, Figure 13 (3rd plot) shows that the HRF for the insurance claims data is monotonically increasing HRF. Due to Figure 14 (top left figure), the reinsurance revenues data are not very skewed and are close to being symmetric, they are of course not completely symmetrical, where the skewness=0.2668196 and the kurtosis=2.264141. No extreme observations are spotted based on Figure 14 (top right and bottom right plots) due to the reinsurance revenues data. Further, Figure 14 (3rd plot) shows that the HRF for the reinsurance revenues data is monotonically increasing.

In this application, we are in the process of a time series of the revenues of reinsurance companies, and we are very interested in knowing the shape of the spread by knowing the extent to which the values of the time series are interconnected with their previous values, and therefore we have drawn the scattergram at lag $k = 1$. The scattergram is a diagram that shows points referencing two different variables. Two variables are observed and plotted on a graph to make a scattergram. The resulting display illustrates how the variables are related. Where the points are most closely grouped together, the link is stronger. Statistical surveys or laboratory test results are occasionally represented using scattergrams. The terms scatter plot, scatter diagram, scatter chart, and scatter graph can all be used to refer to a scattergram. Figure 15 (first row) shows the scattergrams of the insurance claims data. Figure 15 (second row) shows the scattergrams of the reinsurance revenues data.

Moreover, we offer the autocorrelation function (ACF), The autocovariance function (ACOF) and PACF. The ACF shows how the correlation between any two signal values changes as their separation changes. The theoretical ACF provides no information about the process's frequency content; instead, it measures the stochastic process memory in the time domain, it offers some details regarding the distribution of hills and valleys on the surface. The ACOF is defined as the sequence of covariances of a stationary process. The theoretical ACF is given in Figure 16 (tope left plot), the ACOF in Figure 16 (top middle plot) and theoretical PACF in Figure 16 (the 2nd plot) for the insurance claims data data under $lag = k = 1$. The theoretical ACF is given in Figure 16 ($3\,rd$ plot), the ACOF in Figure 16 (bottom middle plot) and theoretical PACF in Figure 16 (the 4th plot) for the reinsurance revenues data under $lag = k = 1$.

Table 14: Summary statistics.

Statistic	Value	
	Insurance claims	Reinsurance revenue
Mean and Variance	7.6858930,0.5444321	32360452,1.355245×10^{14}
Kurtosis and Skewness	2.7884640, −0.748278	2.264141,0.2668196
Dispersion index	0.07083524 (< 1)	4187967 (> 1)
Min and Max	5.828946,8.745603	14021480,58756474
Length and Median	28,7.740188	64,32360452
Quantiles (0.25%,0.75%)	(7.169353,8.281252)	(22426547,39929985)

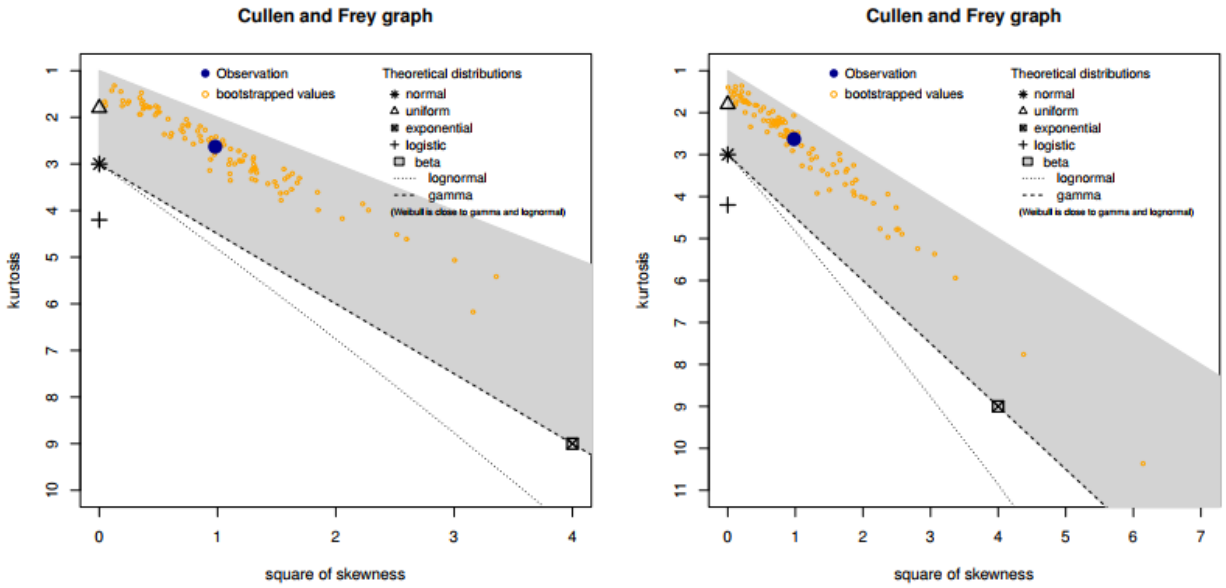

Figure 12: Cullen and Frey plot under the insurance claims (left) reinsurance revenues (right) data sets.

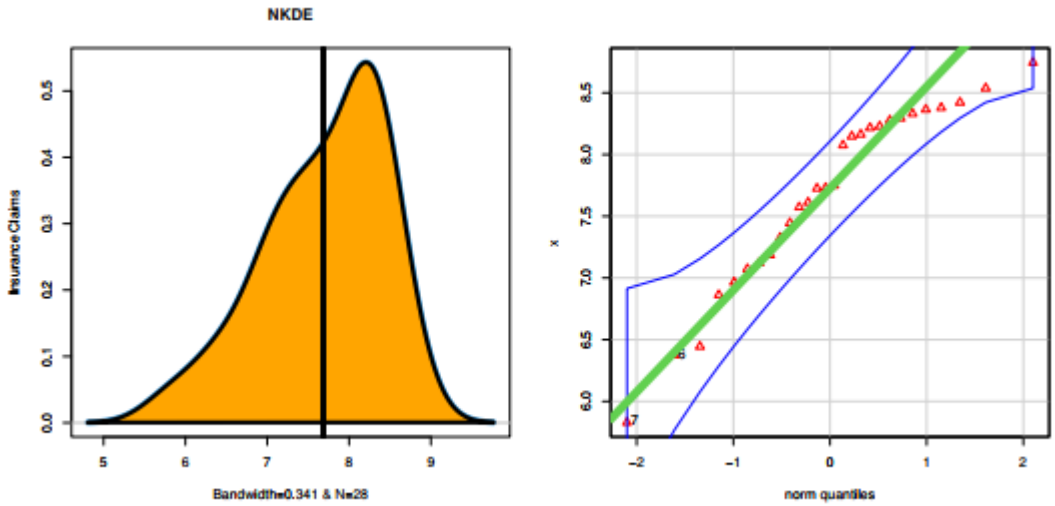

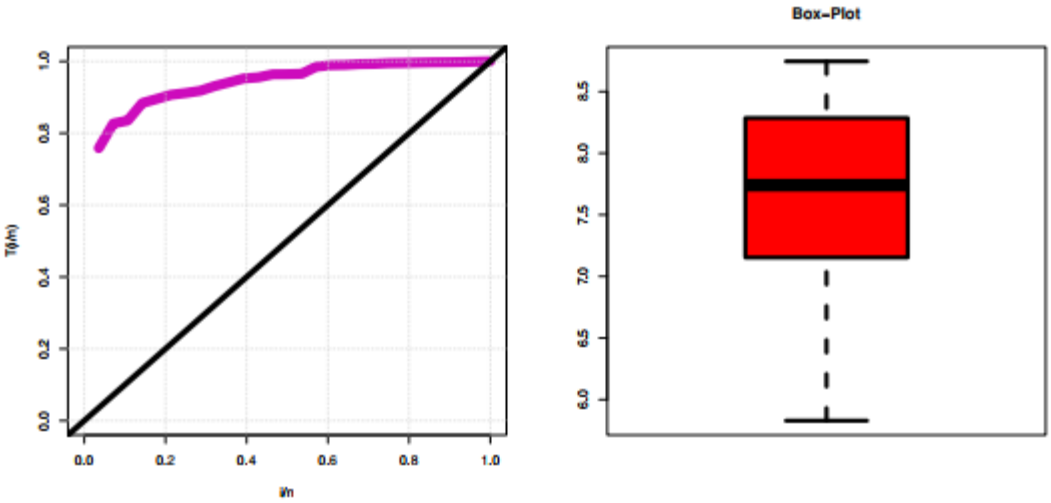

Figure 13: NKDE plot, Q-Q plot, TTT plot and box plot for the insurance claims data.

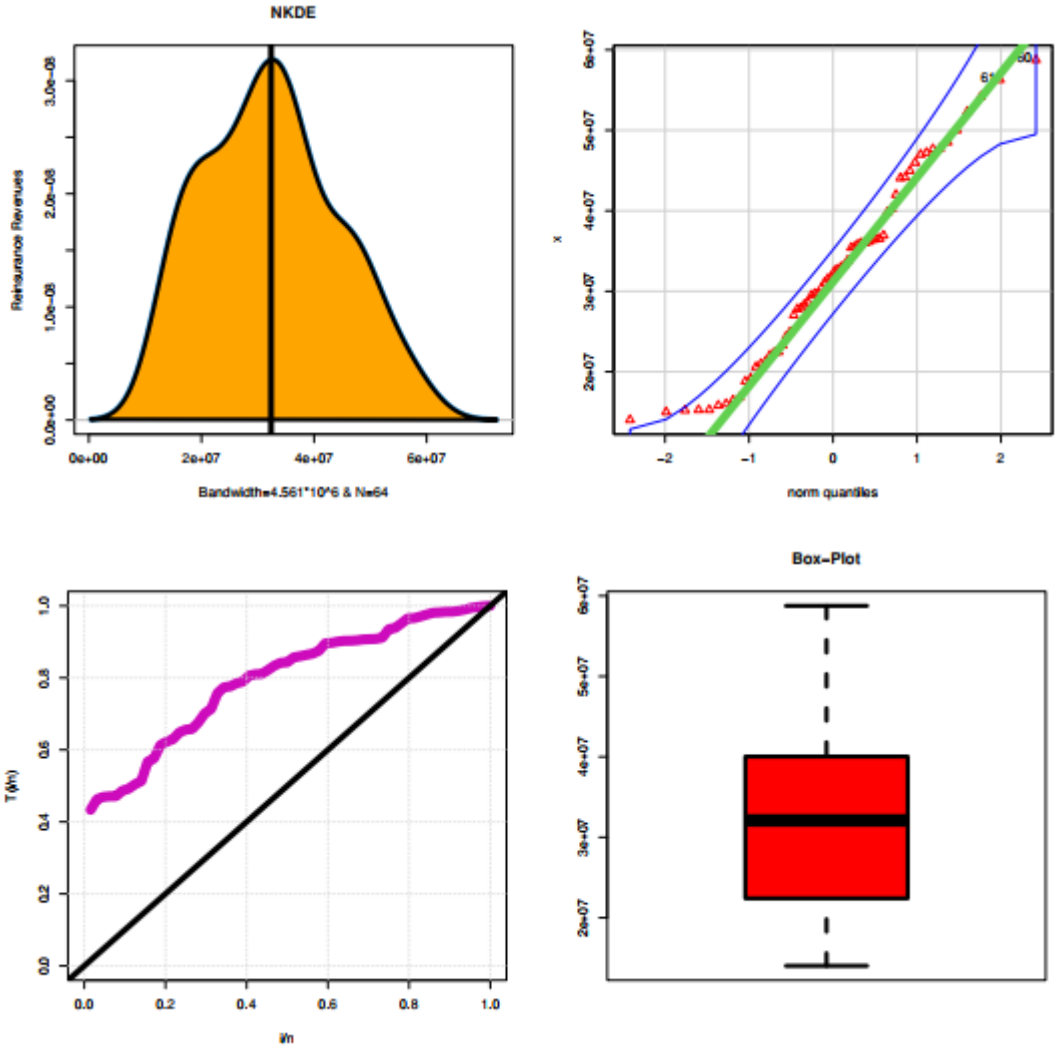

Figure 14: NKDE plot, Q-Q plot, TTT plot and box plot for the reinsurance revenues data.

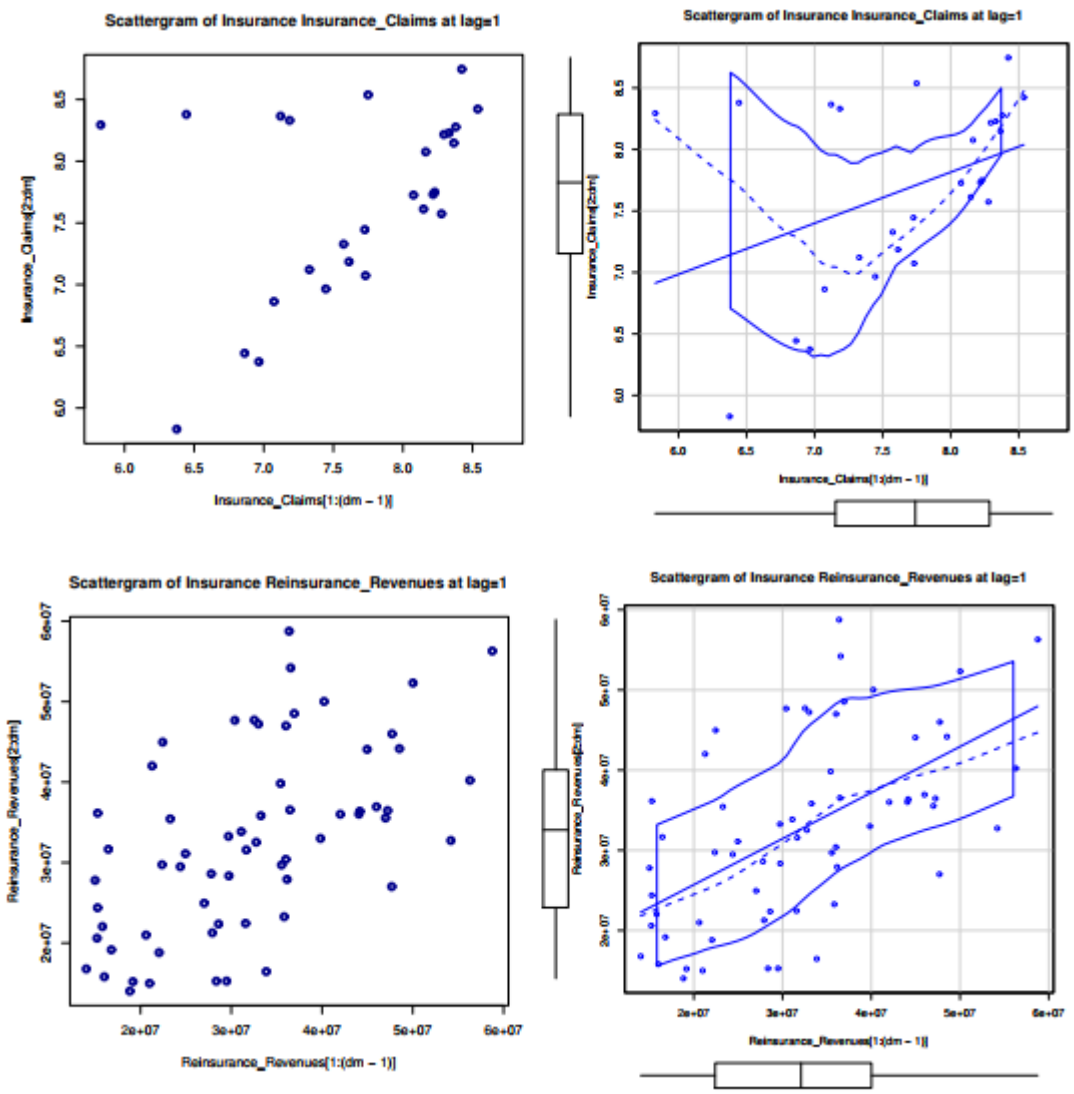

Figure 15: The scattergrams of the insurance claims data (first row)
And the scattergrams of the reinsurance revenues data (second row).

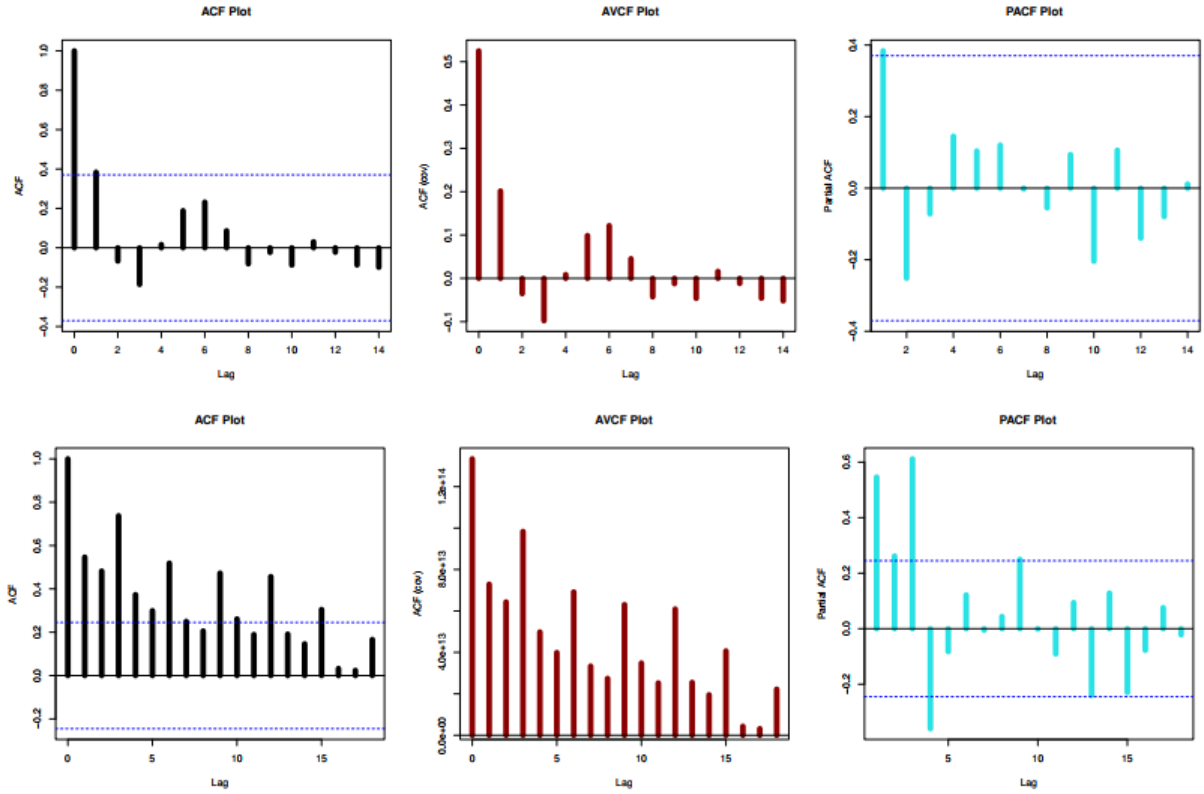

Figure 16: The ACF, ACVF and PACF of the insurance claims data (first row) and the ACF, ACVF and PACF of the reinsurance revenues data (second row).

For the two-insurance data, we propose an application for risk analysis using VaR, TVaR, TV, and TMV metrics. The risk analysis is done for some confidence levels (CLs)

$$\overline{\rho} = 50\%, 40\%, 30\%, 20\%, 10\%, 5\%, 1\%.$$

For the insurance claims data: The five measures are estimated for the GOLLX and XGamma models, the XGamma model is the baseline model for this application. Table 15 reports the KRIs for the GOLLX and XGamma models. For the GOLLX model, the quantity VaR $(X|_{\overline{\rho},\underline{V}})$ ranges from 1.260268$|\,\overline{\rho} = 50\%$ to 5.852501$|\,\overline{\rho} = 1\%$, TVaR $(X|_{\overline{\rho},\underline{V}})$ ranges from 2.981853$|\,\overline{\rho} = 50\%$ to 6.463228$|\,\overline{\rho} = 1\%$, TV $(X|_{\overline{\rho},\underline{V}})$ ranges from 3.891189$|\,\overline{\rho} = 50\%$ to 20.37185$|\,\overline{\rho} = 1\%$ and TMV $(X|_{\overline{\rho},\underline{V}})$ ranges from 6.678482$|\,\overline{\rho} = 50\%$ to 25.81649$|\,\overline{\rho} = 1\%$. For the XGamma model, VaR $(X|_{\overline{\rho},\lambda})$ ranges from 0.6484999$|\,\overline{\rho} = 50\%$ to 1.534491$|\,\overline{\rho} = 1\%$, TVaR $(X|_{\overline{\rho},\lambda})$ ranges from 2.397684$|\,\overline{\rho} = 50\%$ to 3.240351$|\,\overline{\rho} = 1\%$, TV $(X|_{\overline{\rho},\lambda})$ ranges from 3.641414$|\,\overline{\rho} = 50\%$ to 4.046323$|\,\overline{\rho} = 1\%$, and TMV $(X|_{\overline{\rho},\lambda}, 0.95)$ ranges from 5.8570282$|\,\overline{\rho} = 50\%$ to 7.084358$|\,\overline{\rho} = 1\%$. For the reinsurance revenues data: The five measures are estimated for the GOLLX and XGamma models, the XGamma model is the baseline model for this application. Table 16 reports the KRIs for the GOLLX and XGamma models for the reinsurance data. For the GOLLX model, the quantity VaR $(X|_{\overline{\rho},\underline{V}})$ ranges from 2.464745$|\,\overline{\rho} = 50\%$ to 4.979179$|\,\overline{\rho} = 1\%$, TVaR $(X|_{\overline{\rho},\underline{V}})$ ranges from 4.336615$|\,\overline{\rho} = 50\%$ to 4.988936$|\,\overline{\rho} = 1\%$, TV $(X|_{\overline{\rho},\underline{V}})$ ranges from 38.98669$|\,\overline{\rho} = 50\%$ to 71.73617$|\,\overline{\rho} = 1\%$ and TMV $(X|_{\overline{\rho},\underline{V}})$ ranges from 41.37397$|\,\overline{\rho} = 50\%$ to 73.13830$|\,\overline{\rho} = 1\%$. For the XGamma model, VaR $(X|_{\overline{\rho},\lambda})$ ranges from 2.0433$|\,\overline{\rho} = 50\%$ to 3.37588$|\,\overline{\rho} = 1\%$, TVaR $(X|_{\overline{\rho},\lambda})$ ranges from 4.127986$|\,\overline{\rho} = 50\%$ to 4.70335$|\,\overline{\rho} = 1\%$, TV $(X|_{\overline{\rho},\lambda})$ ranges from 35.48$|\,\overline{\rho} = 50\%$ to 48.2822$|\,\overline{\rho} = 1\%$, and TMV $(X|_{\overline{\rho},\lambda}, 0.95)$ ranges from 37.8352$|\,\overline{\rho} = 50\%$ to 50.57139$|\,\overline{\rho} = 1\%$. In general, we find the following outcomes for the two models:

$$\mathrm{VaR}(X|_{\overline{\rho}=50\%}) <\ldots< \mathrm{VaR}(X|_{\overline{\rho}=1\%}), \mathrm{TVaR}(X|_{\overline{\rho}=50\%}) <\ldots< \mathrm{TVaR}(X|_{\overline{\rho}=1\%}),$$

$$\mathrm{TV}(X|_{\overline{\rho}=50\%}) <\ldots< \mathrm{TV}(X|_{\overline{\rho}=1\%}), \mathrm{TMV}(X|_{\overline{\rho}=50\%}) <\ldots< \mathrm{TMV}(X|_{\overline{\rho}=1\%})|_{\pi=0.95},$$

and

$$\mathrm{EL}(X|_{\overline{\rho}=50\%}) > \mathrm{EL}(X|_{\overline{\rho}=40\%}) > \ldots > \mathrm{EL}(X|_{\overline{\rho}=1\%}),$$

It is significant to notice that the mean excess loss function's value, if one exists, has fallen, which may be an indication that reinsurance companies will reach their anticipated profits in the following years. It is significant to observe that the mean excess loss function value has become negative, which may be an indication that reinsurance companies may reach their anticipated earnings in the following years.

In addition, the outcomes of the comparison between the GOLLX and XGamma models are as follows:

- $\forall\ \overline{\rho}$: VaR $(X|_{\rho,\underline{V}})$ for GOLLX model > VaR $(X|_{\overline{\rho},\lambda})$ for XGamma model.
- $\forall\ \overline{\rho}$: TVaR $(X|_{\rho,\underline{V}})$ for GOLLX model > TVaR $(X|_{\overline{\rho},\lambda})$ for XGamma model.
- $\forall\ \overline{\rho}$: TV $(X|_{\rho,\underline{V}})$ for GOLLX model > TV $(X|_{\overline{\rho},\lambda})$ for XGamma model.
- $\forall\ \overline{\rho}$: TMV $(X|_{\rho,\underline{V}}, 0.95)$ for GOLLX model > TMV $(X|_{\overline{\rho},\lambda}, 0.95)$ for XGamma model.
- $\forall\ \overline{\rho}$: VaR $(X|_{\overline{\rho}})$ < TVaR $(X|_{\overline{\rho}})$ < TMV $(X|_{\overline{\rho}})$.

For the insurance claims data: $\forall\ \overline{\rho}$, EL $(X|_{\overline{\rho},\underline{V}})$ is evaluated where for the GOLLX model, t the EL $(X|_{\overline{\rho}})$ decreases as ρ increases and it started with 1.721585 $|_{\overline{\rho}=50\%}$ and ended with 0.61073 $|_{\overline{\rho}=1\%}$. For the XGamma model the EL $(X|_{\overline{\rho},\lambda})$ decreases as ρ increases and it started with 1.749184 $|_{\overline{\rho}=50\%}$ and ended with 1.705860 $|_{\overline{\rho}=1\%}$. EL $(X|_{\overline{\rho},\underline{V}})$ for the GOLLX model < EL $(X|_{\overline{\rho},\lambda})$ for the XGamma model $\forall\ \overline{\rho}$. For the reinsurance revenues data: $\forall\ \overline{\rho}$, EL $(X|_{\overline{\rho},\underline{V}})$ is evaluated where for the GOLLX model, the EL $(X|_{\overline{\rho}})$ decreases as ρ increases and it started with 1.8719 $|_{\overline{\rho}=50\%}$ and ended with 0.00976 $|_{\overline{\rho}=1\%}$. For the XGamma model the EL $(X|_{\overline{\rho},\lambda})$ decreases as ρ increases and it started with 02.084683 $|_{\overline{\rho}=50\%}$ and ended with 1.327465 $|_{\overline{\rho}=1\%}$. EL $(X|_{\overline{\rho},\underline{V}})$ for the GOLLX model < EL $(X|_{\overline{\rho},\lambda})$ for the XGamma model $\forall\ \overline{\rho}$. For $\overline{\rho} = 50\%$, EL $(X|_{\overline{\rho},\underline{V}})$ for the GOLLX model = 1.8718700. For the insurance claims and reinsurance revenues, the mean excess losses under the new model are often lower than their comparable ones under the baseline model. Figure 17 reports the plots of the VaR, TVaR, TV and TMV and the corresponding Cullen and Frey for the new model under the insurance claims. Figure 18 reports the plots of the VaR, TVaR, TV and TMV and the corresponding Cullen and Frey for the new model under the the reinsurance revenues. The first row of each plot provides a graphical comparison between GOLLX and XGamma models. Based on Figure 17 and Figure 18 the GOLLX model has a heavier tail than the XGamma distribution for all KRIs. Therefore, when measuring risk and issues of disclosure, we prefer the model with has a heavier tail.

Table 15: KRIs under the insurance claims data.

	$\overline{\rho}$	VaR$(X\|_{\rho,\underline{V}})$	TVaR$(X\|_{\rho,\underline{V}})$	TV$(X\|_{\rho,\underline{V}})$	TMV$(X\|_{\rho,\underline{V}})$	EL$(X\|_{\rho,\underline{V}})$
GOLLX	50%	1.260268	2.981853	3.891189	6.678482	1.721585
	40%	1.665983	3.363419	4.132600	7.289390	1.697436
	30%	2.189041	3.846229	4.570144	8.187866	1.657188
	20%	2.926251	4.502942	5.538943	9.764937	1.576691
	10%	4.186518	5.521718	8.872839	13.95091	1.335200
	5%	5.446786	6.299004	16.40810	21.88669	0.8522177
	1%	5.852501	6.463228	20.37185	25.81649	0.6107266
XGamma	50%	0.6484999	2.397684	3.641414	5.857028	1.749184
	40%	0.7832417	2.527119	3.686861	6.029637	1.743877
	30%	0.8987206	2.637725	3.729751	6.180988	1.739004
	20%	0.990413	2.725322	3.766610	6.303601	1.734909
	10%	1.188957	2.914258	3.855771	6.577241	1.725301
	5%	1.334489	3.052050	3.930112	6.785656	1.717561
	1%	1.534491	3.240351	4.046323	7.084358	1.705860

Table 16: KRIs under the reinsurance revenues data.

	$\overline{\rho}$	VaR$(X\|_{\rho,\underline{V}})$	TVaR$(X\|_{\rho,\underline{V}})$	TV$(X\|_{\rho,\underline{V}})$	TMV$(X\|_{\rho,\underline{V}})$	EL$(X\|_{\rho,\underline{V}})$
GOLLX	50%	2.464745	2.464745	2.464745	2.464745	2.464745
	40%	2.944219	2.944219	2.944219	2.944219	2.944219
	30%	3.293023	3.293023	3.293023	3.293023	3.293023

	20%	4.097732	4.097732	4.097732	4.097732	4.097732
	10%	4.697656	4.697656	4.697656	4.697656	4.697656
	5%	4.965314	4.965314	4.965314	4.965314	4.965314
	1%	4.979179	4.979179	4.979179	4.979179	4.979179
XGamma	50%	2.043302	2.043302	2.043302	2.043302	2.043302
	40%	2.248476	2.248476	2.248476	2.248476	2.248476
	30%	2.464745	2.464745	2.464745	2.464745	2.464745
	20%	2.693378	2.693378	2.693378	2.693378	2.693378
	10%	3.020090	3.020090	3.020090	3.020090	3.020090
	5%	3.283922	3.283922	3.283922	3.283922	3.283922
	1%	3.375880	3.375880	3.375880	3.375880	3.375880

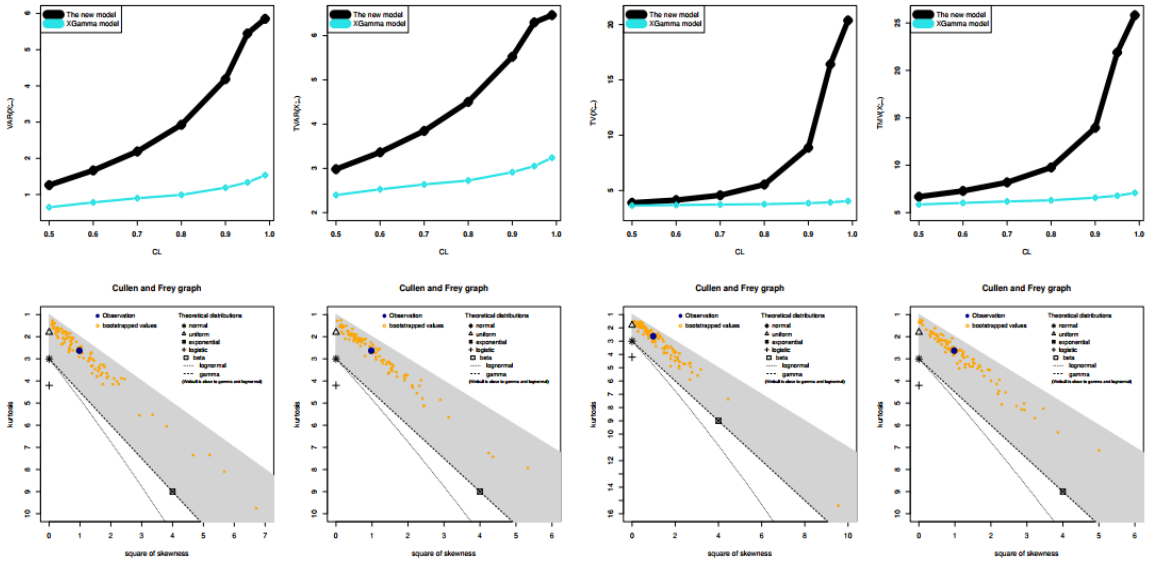

Figure 17: VaR, TVaR, TV and TMV and the corresponding Cullen and Frey for the insurance claims.

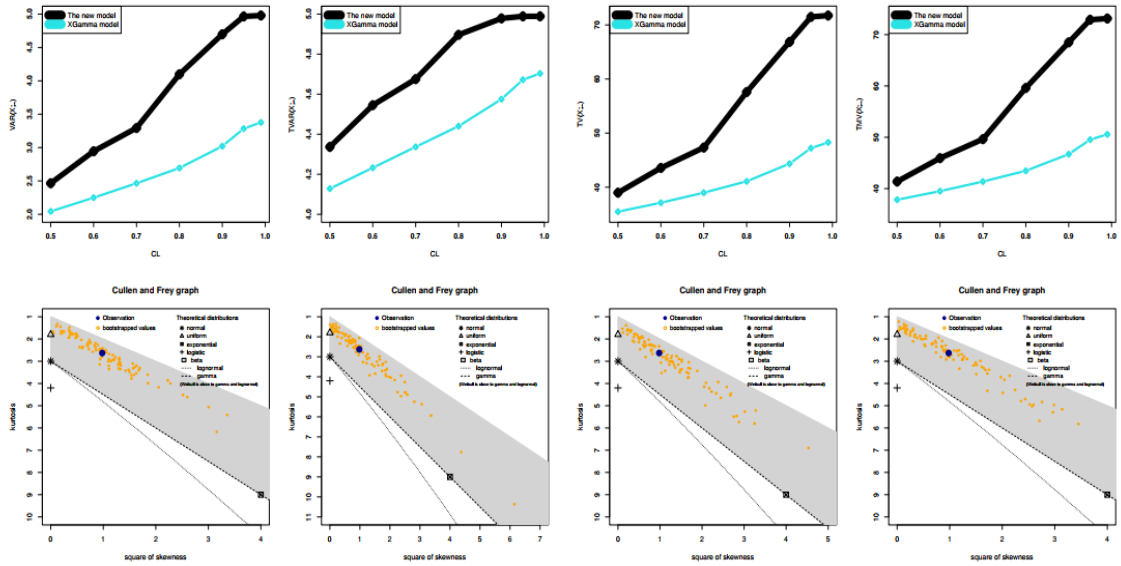

Figure 18: VaR, TVaR, TV and TMV and the corresponding Cullen and Frey for the reinsurance revenues.

6. Simulation design and results for estimation of VaR

This section entails a simulation study to compare the performance of the proposed GOLLX distribution with the existing XGamma distribution of Sen et al. (2016). The comparison would be done in two stages. Firstly, we compare the estimation of the parameter λ using the maximum likelihood estimation technique from the XGamma distribution and the proposed GOLLX distribution. Secondly, we assess the performance of the proposed GOLLX distribution in estimating high quantiles (i.e. VaR) in relation to the existing XGamma distribution. In this subsection, we provide simulation results for estimating high quantiles (VaR). Samples are generated from a mixture of exponential and gamma distributions to obtain samples from the XGamma and GOLLX distributions. Here, the inverses of the distribution's functions are obtained numerically and the estimation of parameters in both cases are done using the ML method. We vary the common shape parameter, λ ($\lambda = 0.5,\ 0.75,\ 1,\ 3.00,\ 6.00$) to both distributions, sample size and the quantile level, q ($q = 0.95,0.99,\ 0.999$). The number of repetitions is fixed at $\hbar = 1000$. Since the results did not differ in terms of the pattern of the performance at different quantile levels, for brevity and ease of presentation, we present the results for $q = 0.99$ only. The results for the estimation of quantiles for samples generated from the GOLLX distribution are presented in Table 17, Table 18, Table 19, Table 20 and Table 21 for corresponding values of the shape parameter λ. Note that the other parameters of the GOLLX are held constant: $\alpha = 9,\ \beta = .51,\ \lambda = 0.5$. It can be seen from these figures that the GOLLX estimation of the high quantile (VaR) yields lesser MSE and bias values than the XGamma estimator except for the case where $\lambda = 0.50$. In the case of samples generated from XGamma distribution, Table 17, Table 18, Table 19, Table 20, the GOLLX estimator of VaR appears unstable for $\lambda \leq 0.75$. However, it possesses lesser bias and MSE for $0.75 < \lambda \leq 3.00$. In addition, the GOLLX estimator is competitive in terms of bias for $\lambda = 6.00$. Generally, as λ increases the bias and MSE values decrease in the results from XGamma and GOLLX distributions. However, empirical consistency was not uniformly achieved in each of these distributions. Therefore, from these results, the GOLLX provides a viable estimator of the VaR (high quantiles) for samples generated from the GOLLX distribution and competitive in the case of samples from the XGamma distribution.

Table 17: Results for samples generated with λ = 0.50.

	$n = 100$	$n = 500$	$n = 1000$
Estimator	Bias, MSE	Bias, MSE	Bias, MSE
XGamma	12.6304,159.81	12.6202,159.4601	12.6229,159.4492
GOLLX	16.4123,2977.60	16.2713,2984.6024	20.8420 5623.9821

Table 18: Results for samples generated with λ = 0.75.

	$n = 100$	$n = 500$	$n = 1000$
Estimator	Bias, MSE	Bias, MSE	Bias, MSE
XGamma	2.0861,4.3375	2.0789,4.3348	2.0695,4.2900
GOLLX	−0.8759,0.7692	−0.8744,0.7676	−0.8771,0.7697

Table 19: Results for samples generated with λ = 1.

	$n = 100$	$n = 500$	$n = 1000$
Estimator	Bias, MSE	Bias, MSE	Bias, MSE
XGamma	2.0861,4.3375	2.0789,4.3348	2.0695,4.2900
GOLLX	−0.8759,0.7692	−0.8744,0.7676	−0.8771,0.7697

Table 20: Results for samples generated with λ = 3.

	$n = 100$	$n = 500$	$n = 1000$
Estimator	Bias, MSE	Bias, MSE	Bias, MSE
XGamma	1.1272,1.2890	1.1514,1.3300	1.1485,1.3216
GOLLX	−0.2685,0.0888	−0.2600,0.1238	−0.2339,0.1819

Table 21: Results for samples generated with λ = 6.

	$n = 100$	$n = 500$	$n = 1000$
Estimator	Bias, MSE	Bias, MSE	Bias, MSE
XGamma	0.6152,0.3842	0.6226,0.3887	0.6223,0.3877
GOLLX	0.5135,30.7312	0.2477,2.4120	0.2393,0.9564

8. PORT-VaR analysis

In our analysis of extreme financial insurance peaks, we integrate and compare the PORT-VaR methodology with the traditional VaR estimation. The PORT-VaR approach, grounded in extreme value theory, offers a dynamic threshold-based framework for identifying rare but high-impact financial outliers. By contrasting it with the more conventional VaR model, known for its static quantile-based cutoff, we aim to assess the precision and responsiveness of each method in capturing tail-risk behavior specific to the asymmetrical nature of our dataset, characterized by left-skewed insurance claim losses and right-skewed reinsurance revenue gains. This comparison underscores the importance of tailoring risk quantification tools to accommodate skewed distributions inherent in insurance and reinsurance data structures.

Table 22 presents the results of the PORT-VaR analysis applied to insurance claims data, expressed in billion USD. As the CL increases from 55% to 95%, the VaR threshold decreases steadily, from 7.73 to 6.40 billion, indicating a shift in the quantile-based boundary for identifying tail events. Correspondingly, the number of claims exceeding each threshold grows from 15 to 26, reflecting the expected increase in tail density as the cut-off descends into deeper quantiles. This behavior suggests a moderate concentration of extreme losses in the upper tail, with a gradually thickening tail profile that aligns with the left-skewed nature of insurance claim distributions observed in the study.

The PORT-VaR analysis reveals a gradual but consistent increase in the number of extreme claims as the confidence level rises, signaling a moderately fat-tailed loss distribution. Insurance firms should calibrate their capital reserves to account for this growing tail risk, particularly under stress scenarios beyond the 90% confidence level. Given that traditional static VaR may underrepresent true exposure in the upper tail, especially for skewed claim distributions, insurers should adopt dynamic, quantile-adjusted thresholds like PORT-VaR for real-time claims surveillance and early warning systems. The detection of increasingly frequent peaks above the VaR threshold suggests that extreme losses are not isolated anomalies. Insurers should incorporate heavy-tail modeling into underwriting strategies to avoid systematic underestimation of high-impact claim events. With the steepest rise in risk concentration observed between the 80–95% confidence levels, insurers may consider structuring reinsurance treaties (e.g., excess-of-loss or stop-loss agreements) to attach near these thresholds, ensuring coverage activates when peak claim exposures become statistically probable.

Figures 19 and 20 provide graphical reinforcement for the quantitative insights presented in Table 22 regarding the PORT-VaRq analysis of insurance claims. Specifically, Figure 19 illustrates the histograms of the claim's distribution across varying confidence levels, with superimposed VaR thresholds and highlighted peaks. These visual cues reveal a progressive accumulation of claims in the upper-left tail, consistent with the increasing number of peaks reported in Table 22 as the VaRq threshold lowers. Complementarily, Figure 20 visualizes the density curves, offering a clearer view of the tail thickness and how claim values cluster beyond specific quantiles.

Table 22: PORT-VaR analysis for insurance claims in billion USD.

CL	VaR	Number of Peaks Above VaR
55%	7.726563	15
60%	7.604576	17
65%	7.503069	18
70%	7.339545	19
75%	7.169353	21
80%	7.092463	22
85%	7.092463	23
90%	6.737170	25
95%	6.399212	26

Table 23 summarizes the same PORT-VaR procedure, but for reinsurance revenues, reported in USD. Here, a more dynamic pattern emerges: the VaR thresholds drop significantly from approximately 30.6 million USD at the 55% level to about 15.3 million USD at the 95% level. In tandem, the number of revenue observations exceeding the VaR grows rapidly from 35 to 61. This increase is not only sharper but more sustained across confidence levels than in the

insurance claims case. The results highlight a heavier and more active upper tail in the revenue distribution, supporting the paper's characterization of right-skewed reinsurance income, where a substantial portion of gains is concentrated in relatively few, high-value outliers.

The reinsurance revenue data demonstrates a sharp and continuous increase in the number of extreme gains across all confidence levels, indicating a highly skewed and volatile income profile. Reinsurers should account for this variability when forecasting revenue and assessing profitability under uncertainty. The presence of a high frequency of extreme revenue peaks suggests that standard pricing models may fail to capture the nonlinear accumulation of gains. Reinsurers are advised to implement pricing mechanisms that dynamically adjust based on real-time tail behavior and peak clustering patterns. Given the amplified exposure to large, discrete inflows, firms should consider deploying flexible capital allocation strategies that can rapidly respond to windfall scenarios without distorting solvency assessments or internal return targets. Since the PORT-VaR approach provides granular insights into the threshold at which large revenues emerge, reinsurance companies can use this data-driven intelligence to fine-tune the design of retrocession contracts, adjust risk appetite profiles, and strategically select portfolios with favorable skewness properties.

On the other hand, Figures 21 and 22 correspond to the PORT-VaRq analysis of reinsurance revenues as reported in Table 23. Figure 21 displays the histograms with revenue data, emphasizing the significant presence of high-value outliers above the VaRq threshold. This visually aligns with the higher peak counts across confidence levels in Table 23. Figure 22 presents density plots that further affirm the right-skewed structure of the revenue distribution, highlighting a heavier upper tail and more frequent extreme values—critical observations that validate the quantitative escalation in peaks and the need for adaptive risk strategies.

Table 23: PORT-VaR analysis for reinsurance revenues in USD.

CL	VaR	Number of Peaks Above VaR
55%	30643375	35
60%	29529133	38
65%	27936937	41
70%	24892526	45
75%	22426547	48
80%	21160380	51
85%	18970872	54
90%	16143451	59
95%	15265431	61

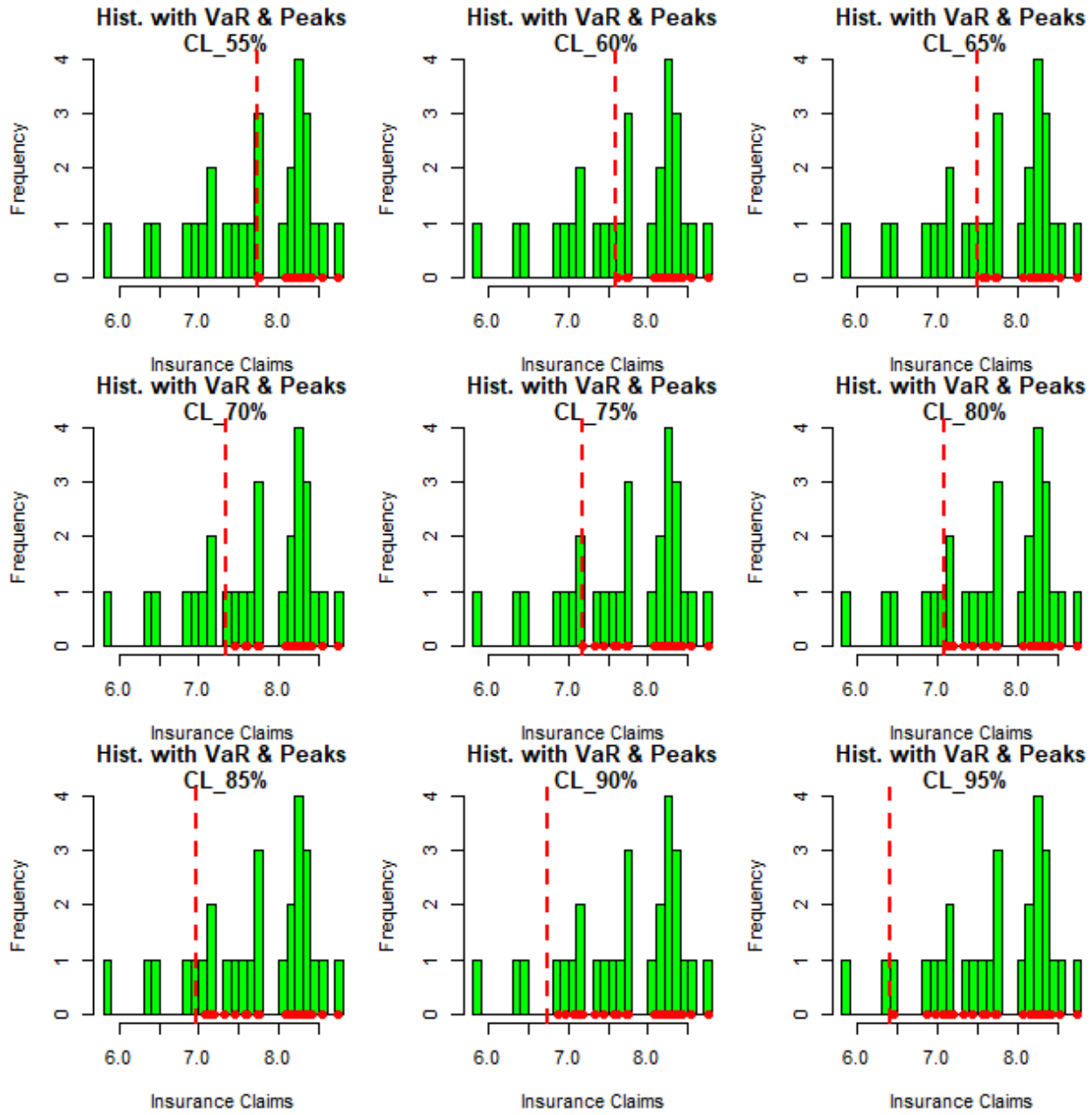

Figure 19: Histograms with VaR and peaks under the insurance claims.

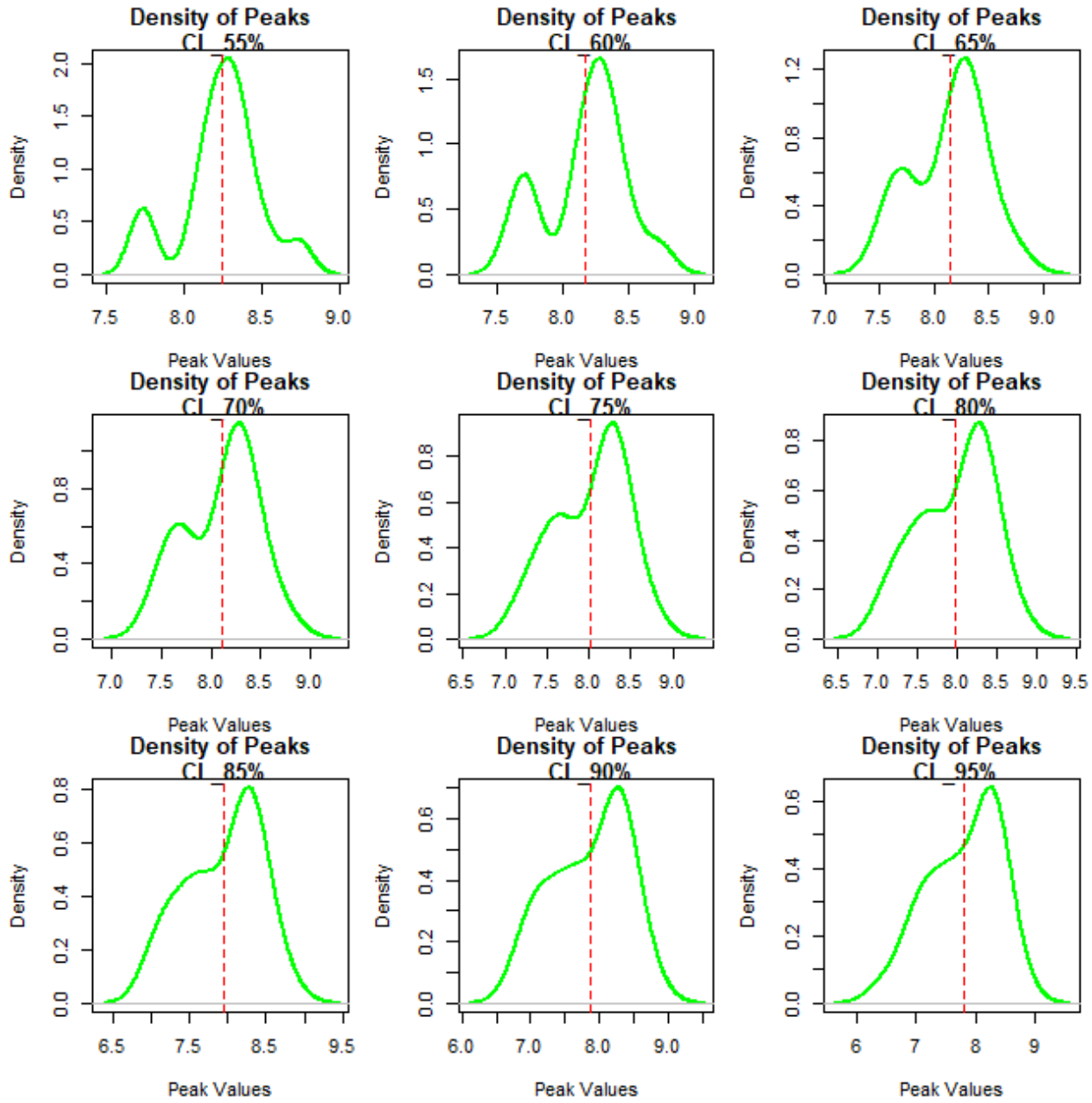

Figure 20: Densities with VaR and peaks under the insurance claims.

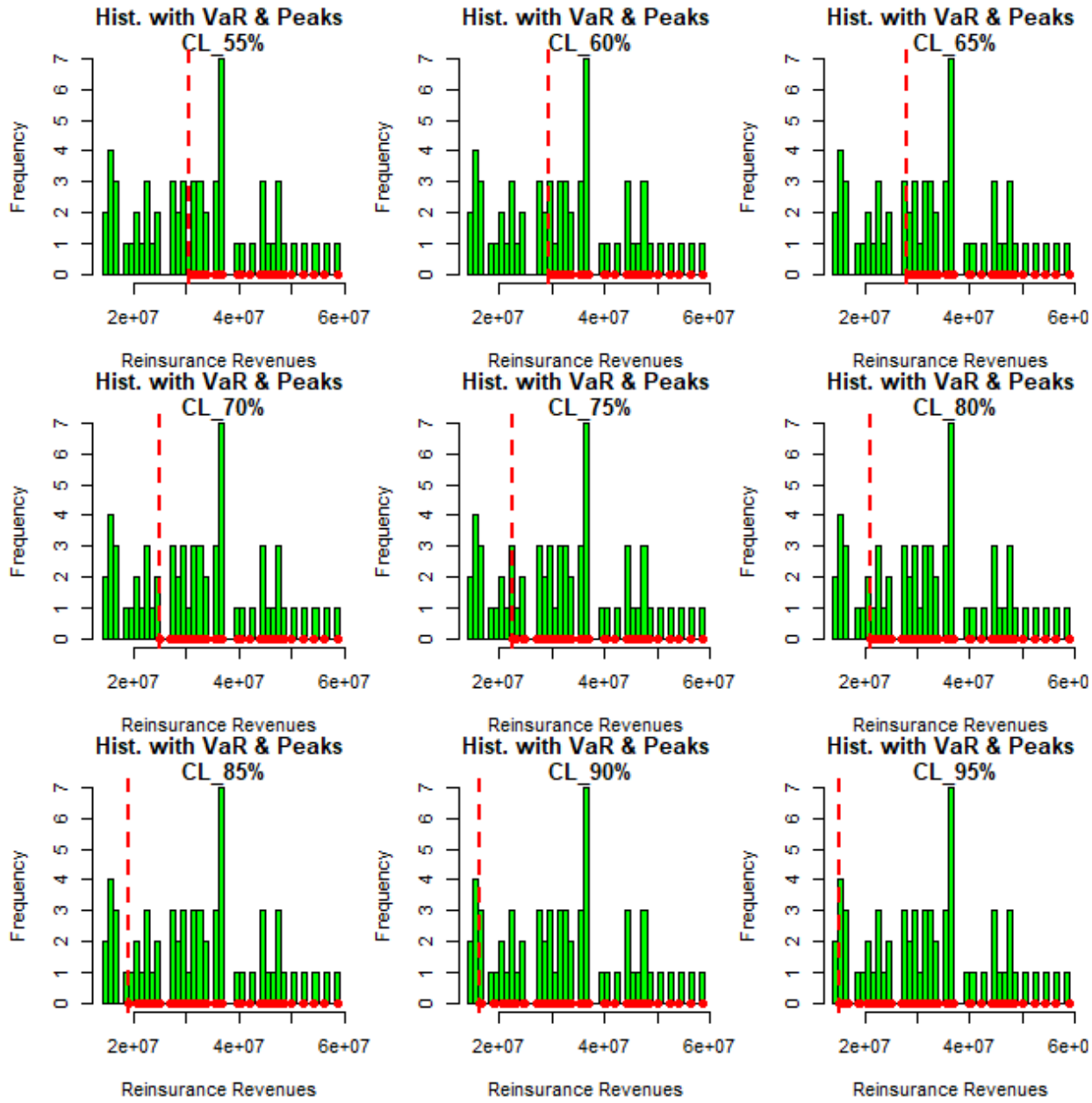

Figure 21: Histograms with VaR and peaks under the reinsurance data.

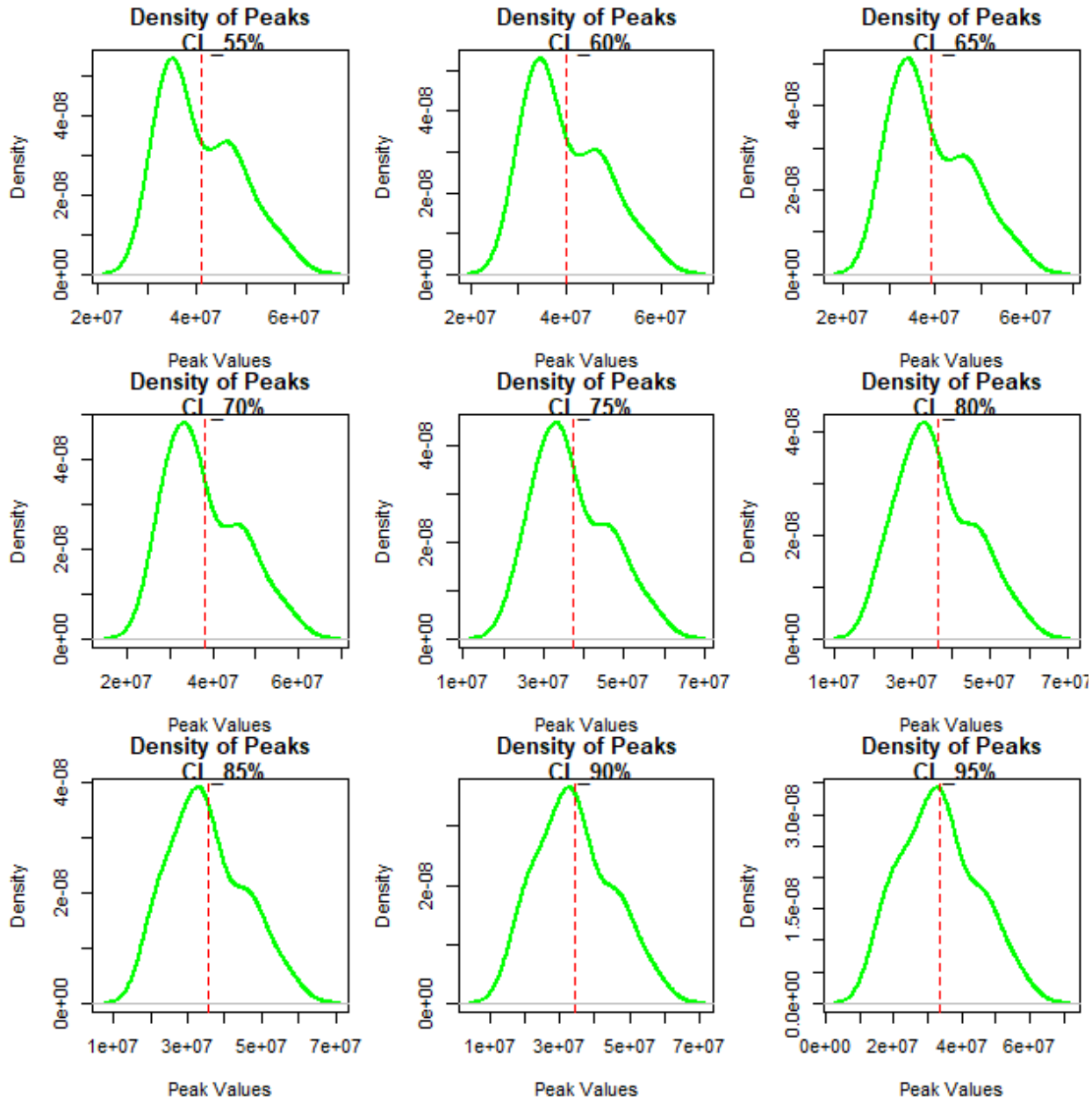

Figure 22: Densities with VaR and peaks under the reinsurance data.

8. Concluding remarks and discussion

The continuous probability distributions can be successfully utilized to characterize and evaluate the risk exposure in applied actuarial analysis. Actuaries often prefer to convey the level of exposure to a certain hazard using merely a numerical value, or at the very least, a small number of numbers. In this paper, a new applied probability model was presented and used to model six different sets of data. About estimating the risks that insurance companies are exposed to and the revenues of the reinsurance process, we have analyzed and studied data on insurance claims and data on reinsurance revenues as an actuarial example. These actuarial risk exposure functions, sometimes referred to as main risk actuarial indicators, are unquestionably a result of a particular model that can be explained. Five crucial actuarial indicators are used in this study to identify the risk exposure in insurance claims and reinsurance revenues. We develop a new XGamma model specifically for this application. The parameters were estimated using the maximum-likelihood technique, maximum product spacing, and least square estimation. Monte Carlo simulation research is conducted under a specific set of conditions and controls. Additionally, five risk indicators -value-at-risk, tail-variance, tail value-at-risk, tail mean-variance, and mean of the excess loss function- were utilized to explain the risk exposure in the

context of data on insurance claims and reinsurance revenue. The peak-over-random-threshold mean-of-order-p approach and value-at-risk estimate are considered and contrasted through controlled and comprehensive groups of simulation studies under certain conditions. For the insurance claims data under the new model, the following results can be shown:

I. The quantity VaR $(X|_{\overline{\rho},\underline{V}})$ ranges from 1.260268$|\ \overline{\rho} = 50\%$ to 5.852501$|\ \overline{\rho} = 1\%$. However, for the baseline model, VaR $(X|_{\overline{\rho},\lambda}) \in$ (0.6484999$|\ \overline{\rho} = 50\%$, 1.534491$|\ \overline{\rho} = 1\%$).

II. TVaR $(X|_{\overline{\rho},\underline{V}})$ ranges from 2.981853$|\ \overline{\rho} = 50\%$ to 6.463228$|\ \overline{\rho} = 1\%$. However, for the baseline model, TVaR $(X|_{\overline{\rho},\lambda}) \in$ (2.397684$|\ \overline{\rho} = 50\%$, 3.240351$|\ \overline{\rho} = 1\%$).

III. TV $(X|_{\overline{\rho},\underline{V}})$ ranges from 3.891189$|\ \overline{\rho} = 50\%$ to 20.37185$|\ \overline{\rho} = 1\%$. However, for the baseline model, TV $(X|_{\overline{\rho},\lambda}) \in$ (3.641414$|\ \overline{\rho} = 50\%$, 4.046323$|\ \overline{\rho} = 1\%$).

IV. TMV $(X|_{\overline{\rho},\underline{V}})$ ranges from 6.678482$|\ \overline{\rho} = 50\%$ to 25.81649$|\ \overline{\rho} = 1\%$. However, for the baseline model, TMV $(X|_{\overline{\rho},\lambda}, 0.95) \in$ (5.8570282$|\ \overline{\rho} = 50\%$, 7.084358$|\ \overline{\rho} = 1\%$).

For the reinsurance revenues data under the new model, the following results can be highlighted:

I. The quantity VaR $(X|_{\overline{\rho},\underline{V}})$ ranges from 2.464745$|\ \overline{\rho} = 50\%$ to 4.979179$|\ \overline{\rho} = 1\%$. However, for the baseline model, VaR $(X|_{\overline{\rho},\lambda}) \in$ (2.0433$|\ \overline{\rho} = 50\%$, 3.37588$|\ \overline{\rho} = 1\%$) .

II. TVaR $(X|_{\overline{\rho},\underline{V}})$ ranges from 4.336615$|\ \overline{\rho} = 50\%$ to 4.988936$|\ \overline{\rho} = 1\%$. However, for the baseline model, TVaR $(X|_{\overline{\rho},\lambda}) \in$ (4.127986$|\ \overline{\rho} = 50\%$, 4.70335$|\ \overline{\rho} = 1\%$).

III. TV $(X|_{\overline{\rho},\underline{V}})$ ranges from 38.98669$|\ \overline{\rho} = 50\%$ to 71.73617$|\ \overline{\rho} = 1\%$. However, for the baseline model, TV $(X|_{\overline{\rho},\lambda}) \in$ (35.48$|\ \overline{\rho} = 50\%$ to 48.2822$|\ \overline{\rho} = 1\%$).

IV. TMV $(X|_{\overline{\rho},\underline{V}})$ ranges from 41.37397$|\ \overline{\rho} = 50\%$ to 73.13830$|\ \overline{\rho} = 1\%$. However, for the baseline model, TMV $(X|_{\overline{\rho},\lambda}, 0.95) \in$ (37.8352$|\ \overline{\rho} = 50\%$, 50.57139$|\ \overline{\rho} = 1\%$).

References

1. Abonongo, J., Abonongo, A. I. L., Aljadani, A., Mansour, M. M., & Yousof, H. M. (2025). Accelerated failure model with empirical analysis and application to colon cancer data: Testing and validation. Alexandria Engineering Journal, 113, 391-408.
2. Acerbi, C. and Tasche, D. (2002), On the coherence of expected shortfall, Journal of Banking and Finance, 26, 1487-1503.
3. Alizadeh, M., Afshari, M., Contreras-Reyes, J. E., Mazarei, D., & Yousof, H. M. (2024). The Extended Gompertz Model: Applications, Mean of Order P Assessment and Statistical Threshold Risk Analysis Based on Extreme Stresses Data. IEEE Transactions on Reliability, doi: 10.1109/TR.2024.3425278.
4. Alizadeh, M., Afshari, M., Contreras-Reyes, J. E., Mazarei, D., & Yousof, H. M. (2024). The Extended Gompertz Model: Applications, Mean of Order P Assessment and Statistical Threshold Risk Analysis Based on Extreme Stresses Data. IEEE Transactions on Reliability, doi: 10.1109/TR.2024.3425278.
5. Alizadeh, M., Afshari, M., Cordeiro, G. M., Ramaki, Z., Contreras-Reyes, J. E., Dirnik, F., & Yousof, H. M. (2025). A New Weighted Lindley Model with Applications to Extreme Historical Insurance Claims. Stats, 8 (1), 8.
6. Alizadeh, M., Afshari, M., Cordeiro, G. M., Ramaki, Z., Contreras-Reyes, J. E., Dirnik, F., & Yousof, H. M. (2025). A New Weighted Lindley Model with Applications to Extreme Historical Insurance Claims. Stats, 8(1), 8.
7. Alizadeh, M., Afshari, M., Ranjbar, V., Merovci, F. and Yousof, H. M. (2023). A novel XGamma extension: applications and actuarial risk analysis under the reinsurance data. São Paulo Journal of Mathematical Sciences, 1-31.
8. Aljadani, A., Mansour, M. M., & Yousof, H. M. (2024). A Novel Model for Finance and Reliability Applications: Theory, Practices and Financial Peaks Over a Random Threshold Value-at-Risk Analysis. Pakistan Journal of Statistics and Operation Research, 20(3), 489-515. https://doi.org/10.18187/pjsor.v20i3.4439
9. AlKhayyat, S. L., Haitham M. Yousof, Hafida Goual, Hamida, T., Hamed, M. S., Hiba, A., & Mohamed Ibrahim. (2025). Rao-Robson-Nikulin Goodness-of-fit Test Statistic for Censored and Uncensored Real Data with Classical and Bayesian Estimation. Statistics, Optimization & Information Computing. https://doi.org/10.19139/soic-2310-5070-1710
10. Artzner, P. (1999). Application of coherent risk measures to capital requirements in insurance. N. Am. Actuar. J., 3, 11--25.
11. Bantan, R., Hassan, A. S., Elsehetry, M. and Kibria, B. M. (2020). Half-logistic XGamma distribution: Properties and estimation under censored samples. Discrete Dynamics in Nature and Society, 2020.
12. Charpentier, A. (2014). Computational actuarial science with R. CRC press.

13. Chen M., H., & Shao Q. M., (1999). Monte Carlo estimation of Bayesian credible and HPD intervals. Journal of Computational and Graphical Statistics, 8 (1), 69-92.
14. Cordeiro, G. M., Altun, E., Korkmaz, M. C., Pescim, R. R. and Afify, A. Z. and Yousof, H. M. (2020). The XGamma Family: Censored Regression Modelling and Applications. Revstat Statistical Journal, 18 (5), 593--612.
15. Das, J., Hazarika, P. J., Alizadeh, M., Contreras-Reyes, J. E., Mohammad, H. H., & Yousof, H. M. (2025). Economic Peaks and Value-at-Risk Analysis: A Novel Approach Using the Laplace Distribution for House Prices. Mathematical and Computational Applications, 30(1), 4.
16. Das, J., Hazarika, P. J., Alizadeh, M., Contreras-Reyes, J. E., Mohammad, H. H., & Yousof, H. M. (2025). Economic Peaks and Value-at-Risk Analysis: A Novel Approach Using the Laplace Distribution for House Prices. Mathematical and Computational Applications, 30(1), 4.
17. Elbatal, I., Diab, L. S., Ghorbal, A. B., Yousof, H. M., Elgarhy, M. and Ali, E. I. (2024). A new losses (revenues) probability model with entropy analysis, applications and case studies for value-at-risk modeling and mean of order-P analysis. AIMS Mathematics, 9 (3), 7169-7211.
18. Feigl, P. and Zelen, M. (1965). Estimation of exponential survival probabilities with concomitant information. Biometrics, 4, 826-838.
19. Furman, E., Landsman, Z. (2006). Tail variance premium with applications for elliptical portfolio of risks. ASTIN Bulletin, 36 (2), 433—462
20. Gleaton, J. U. and Lynch, J. D. (2004). On the distribution of the breaking strain of a bundle of brittle elastic fibers. Adv. Appl. Probab. 36, 98--115.
21. Gleaton, J. U. and Lynch, J. D. (2006). Properties of generalized log-logistic families of lifetime distributions. J. Probab. Stat. Sci. 4, 51-64.
22. Gleaton, J. U. and Lynch, J. D. (2010). Extended generalized log-logistic families of lifetime distributions with an application. J. Probab. Stat. Sci. 8, 1-17.
23. Hafiz, U. A., Salleh, F., Garba, M. and Rashid, N. (2021). Projecting insurance penetration rate in Nigeria: An ARIMA approach. REVISTA GEINTEC-GESTAO INOVACAO ETECNOLOGIAS, 11 (3), 63-75.
24. Hamed, M. S., Cordeiro, G. M. and Yousof, H. M. (2022). A New Compound Lomax Model: Properties, Copulas, Modeling and Risk Analysis Utilizing the Negatively Skewed Insurance Claims Data. Pakistan Journal of Statistics and Operation Research, 18 (3), 601-631. https://doi.org/10.18187/pjsor.v18i3.3652
25. Hamedani, G. G., Goual, H., Emam, W., Tashkandy, Y., Ahmad Bhatti, F., Ibrahim, M. and Yousof, H. M. (2023). A new right-skewed one-parameter distribution with mathematical characterizations, distributional validation, and actuarial risk analysis, with applications. Symmetry, 15 (7), 1297.
26. Hashempour, M., Alizadeh, M., & Yousof, H. (2024). The Weighted Xgamma Model: Estimation, Risk Analysis and Applications. Statistics, Optimization & Information Computing, 12(6), 1573-1600.
27. Hashempour, M., Alizadeh, M., & Yousof, H. (2024a). The Weighted Xgamma Model: Estimation, Risk Analysis and Applications. Statistics, Optimization & Information Computing, 12 (6), 1573-1600.
28. Hashempour, M., Alizadeh, M., & Yousof, H. M. (2024b). A new Lindley extension: estimation, risk assessment and analysis under bimodal right skewed precipitation data. Annals of Data Science, 11 (6), 1919-1958.
29. Hogg, R.V. and Klugman, S.A., 1984, Loss Distributions (New York: John Wiley & Sons, Inc.).
30. Ibragimov, R. and Prokhorov, A. (2017). Heavy Tails and Copulas: Topics in Dependence Modelling in Economics and Finance; World Scientific: Singapore.
31. Ibrahim, M., Al-Nefaie, A. H., AboAlkhair, A. M., Yousof, H. M., & Ahmed, B. (2025). Modeling Medical and Reliability Data Sets Using a Novel Reciprocal Weibull Distribution: Estimation Methods and Sequential Sampling Plan Based on Truncated Life Testing. Statistics, Optimization & Information Computing.
32. Ibrahim, M., Ansari, S. I., Al-Nefaie, A. H., & Yousof, H. M. (2025). A New Version of the Inverse Weibull Model with Properties, Applications and Different Methods of Estimation. Statistics, Optimization & Information Computing, 13(3), 1120-1143. https://doi.org/10.19139/soic-2310-5070-1658
33. Ibrahim, M., Ansari, S. I., Al-Nefaie, A. H., AboAlkhair, A. M., Hamed, M. S., & Yousof, H. M. (2025). A Novel Fréchet-Poisson Model: Properties, Applications under Extreme Reliability Data, Different Estimation Methods and Case Study on Strength-Stress Reliability Analysis. Statistics, Optimization & Information Computing.
34. Ibrahim, M., Butt, N. S., Al-Nefaie, A. H., Hamedani, G. G., Yousof, H. M., & Mahmoud, A. S. (2025). An Extended Discrete Model for Actuarial Data and Value at Risk Analysis: Properties, Applications and Risk Analysis under Financial Automobile Claims Data. Statistics, Optimization & Information Computing, 13 (1), 27-46.
35. Ibrahim, M., Butt, N. S., Al-Nefaie, A. H., Hamedani, G. G., Yousof, H. M., & Mahmoud, A. S. (2025). An Extended Discrete Model for Actuarial Data and Value at Risk Analysis: Properties, Applications and Risk Analysis under Financial Automobile Claims Data. Statistics, Optimization & Information Computing, 13(1), 27-46.
36. Ibrahim, M.; Emam, W.; Tashkandy, Y.; Ali, M.M.; Yousof, H.M. (2023). Bayesian and Non-Bayesian Risk Analysis

and Assessment under Left-Skewed Insurance Data and a Novel Compound Reciprocal Rayleigh Extension. Mathematics 2023, 11, 1593. https://doi.org/10.3390/ math11071593

37. Khedr, A. M., Nofal, Z. M., El Gebaly, Y. M. and Yousof, H. M. (2023). A Novel Family of Compound Probability Distributions: Properties, Copulas, Risk Analysis and Assessment under a Reinsurance Revenues Data Set. Thailand Statistician, forthcoming.
38. Korkmaz, M. Ç., Altun, E., Yousof, H. M., Afify, A. Z. and Nadarajah, S. (2018). The Burr X Pareto Distribution: Properties, Applications and VaR Estimation. Journal of Risk and Financial Management, 11 (1), 1.
39. Korkmaz, M. Ç., Yousof, H. M., & Ali, M. M. (2017). Some theoretical and computational aspects of the odd Lindley Fréchet distribution. İstatistikçiler Dergisi: İstatistik ve Aktüerya, 10(2), 129-140.
40. Kumar, V. S., Satpathi, D. K., Kumar, P. P. and Haragopal, V. V. (2020). Forecasting motor insurance claim amount using ARIMA model. In AIP Conference Proceedings (Vol. 2246, No. 1, p. 020005). AIP Publishing LLC.
41. Landsman, Z. (2010). On the tail mean--variance optimal portfolio selection. Insur. Math. Econ., 46, 547--553.
42. Lane, M. N. (2000). Pricing risk transfer transactions 1. ASTIN Bull. J. IAA, 30, 259--293.
43. Lindley, D.V. (1958). Fiducial distributions and Bayesian theorem. Journal of the Royal Statistical Society B, 20, 102-107.
44. Loubna, H., Goual, H., Alghamdi, F. M., Mustafa, M. S., Tekle Mekiso, G., Ali, M. M., ... & Yousof, H. M. (2024). The quasi-xgamma frailty model with survival analysis under heterogeneity problem, validation testing, and risk analysis for emergency care data. Scientific Reports, 14 (1), 8973.
45. Merovci, F., Yousof, H. M., & Hamedani, G. G. (2020). The Poisson Topp Leone Generator of Distributions for Lifetime Data: Theory, Characterizations and Applications. Pakistan Journal of Statistics and Operation Research, 16 (2), 343-355. https://doi.org/10.18187/pjsor.v16i2.3230
46. Mohamed, H. S., Cordeiro, G. M. and Yousof, H. M. (2022). The synthetic autoregressive model for the insurance claims payment data: modeling and future prediction. Statistics, Optimization & Information Computing, forthcoming.
47. Mohamed, H. S., Cordeiro, G. M., Minkah, R., Yousof, H. M., & Ibrahim, M. (2024). A size-of-loss model for the negatively skewed insurance claims data: applications, risk analysis using different methods and statistical forecasting. Journal of Applied Statistics, 51 (2), 348-369.
48. Mohammadi, H. and Rich, D. P. (2013). Dynamics of unemployment insurance claims: an application of ARIMA-GARCH models. Atlantic Economic Journal, 41 (4), 413-425.
49. Murthy, D. P., Xie, M., & Jiang, R. (2004). Weibull models. John Wiley & Sons.
50. Nadarajah, S., Bakouch, H. S., & Tahmasbi, R. (2011). A generalized Lindley distribution. Sankhya B, 73, 331-359.
51. Para, B. A., Jan, T. R. and Bakouch, H. S. (2020). Poisson XGamma distribution: A discrete model for count data analysis. Model Assisted Statistics and Applications, 15 (2), 139-151.
52. Ramaki, Z., Alizadeh, M., Tahmasebi, S., Afshari, M., Contreras-Reyes, J. E., & Yousof, H. M. (2025). The Weighted Flexible Weibull Model: Properties, Applications, and Analysis for Extreme Events. Mathematical and Computational Applications, 30(2), 42.
53. Rasekhi, M., Altun, E., Alizadeh, M. and Yousof, H. M. (2022). The Odd Log-Logistic Weibull-G Family of Distributions with Regression and Financial Risk Models. Journal of the Operations Research Society of China, 10(1), 133-158.
54. Salem, M., Emam, W., Tashkandy, Y., Ibrahim, M., Ali, M. M., Goual, H. and Yousof, H. M. (2023). A new lomax extension: Properties, risk analysis, censored and complete goodness-of-fit validation testing under left-skewed insurance, reliability and medical data. Symmetry, 15 (7), 1356.
55. Sen, S., Korkmaz, M. C. and Yousof, H. M. (2018). The quasi XGamma-Poisson distribution. ISTATISTIK: JOURNAL OF THE TURKISH STATISTICAL ASSOCIATION, 11 (3), 65-76.
56. Sen, S., Maiti, S. S. and Chandra, N. (2016). The XGamma Distribution: Statistical Properties and Application. Journal of Modern Applied Statistical Methods, 15 (1), 774--788.
57. Sharma V, Singh S, Singh U. & Agiwal V. (2015). The inverse Lindley distribution: a stress-strength reliability model with applications to head and neck cancer data. *Journal of Industrial and Production Engineering* (2015). 32, 3, 162-173.
58. Shrahili, M., Elbatal, I. and Yousof, H. M. (2021). Asymmetric Density for Risk Claim-Size Data: Prediction and Bimodal Data Applications. Symmetry 2021, 13, 2357.
59. Stein, J. D., Lum, F., Lee, P. P., Rich III, W. L. and Coleman, A. L. (2014). Use of health care claims data to study patients with ophthalmologic conditions. Ophthalmology, 121, 1134-1141.
60. Tasche, D. (2002). Expected Shortfall and Beyond, Journal of Banking and Finance, 26, 1519-1533.
61. Venezian, E. C. and Leng, C. C. (2006). Application of spectral and ARIMA analysis to combined-ratio patterns. The Journal of Risk Finance.
62. Wirch J. (1999). Raising Value at Risk,North American Actuarial Journal, 3, 106-115.

63. Yadav, A. S., Maiti, S. S. and Saha, M. (2021). The inverse XGamma distribution: statistical properties and different methods of estimation. Annals of Data Science, 8 (2), 275-293.
64. Yadav, A. S., Saha, M., Tripathi, H., Kumar, S. (2021). The exponentiated XGamma distribution: a new monotone failure rate model and its applications to lifetime data. Statistica, 81 (3), 303-334.
65. Yadav, A. S., Shukla, S., Goual, H., Saha, M. and Yousof, H. M. (2022). Validation of XGamma exponential model via Nikulin-Rao-Robson goodness-of- fit test under complete and censored sample with different methods of estimation. Statistics, Optimization & Information Computing, 10(2), 457-483.
66. Yousof, H. M., Aljadani, A., Mansour, M. M., & Abd Elrazik, E. M. (2024a). A New Pareto Model: Risk Application, Reliability MOOP and PORT Value-at-Risk Analysis. Pakistan Journal of Statistics and Operation Research, 20(3), 383-407. https://doi.org/10.18187/pjsor.v20i3.4151
67. Yousof, H. M., Ansari, S. I., Tashkandy, Y., Emam, W., Ali, M. M., Ibrahim, M., Alkhayyat, S. L. (2023a). Risk Analysis and Estimation of a Bimodal Heavy-Tailed Burr XII Model in Insurance Data: Exploring Multiple Methods and Applications. Mathematics. 2023; 11 (9):2179. https://doi.org/10.3390/math11092179
68. Yousof, H. M., Saber, M. M., Al-Nefaie, A. H., Butt, N. S., Ibrahim, M. and Alkhayyat, S. L. (2024b). A discrete claims-model for the inflated and over-dispersed automobile claims frequencies data: Applications and actuarial risk analysis. Pakistan Journal of Statistics and Operation Research, 261-284.
69. Yousof, H.M.; Emam, W.; Tashkandy, Y.; Ali, M.M.; Minkah, R.; Ibrahim, M. (2023b). A Novel Model for Quantitative Risk Assessment under Claim-Size Data with Bimodal and Symmetric Data Modeling. Mathematics 2023, 11, 1284. https://doi.org/10.3390/math11061284
70. Yousof, H.M.; Tashkandy, Y.; Emam, W.; Ali, M.M.; Ibrahim, M. (2023c). A New Reciprocal Weibull Extension for Modeling Extreme Values with Risk Analysis under Insurance Data. Mathematics 2023, 11, 966. https://doi.org/10.3390/ math11040966